

Unified Performance Analysis of Reconfigurable Intelligent Surface Empowered Free-Space Optical Communications

Vinay Kumar Chapala, *Graduate Student Member, IEEE* and S. M. Zafaruddin, *Senior Member, IEEE*

Abstract—Reconfigurable intelligent surface (RIS) is an excellent use case for line-of-sight (LOS) based technologies such as free-space optical (FSO) communications. In this paper, we analyze the performance of RIS-empowered FSO (RISE-FSO) systems by unifying Fisher–Snedecor (\mathcal{F}), Gamma-Gamma (\mathcal{GG}), and Málaga (\mathcal{M}) distributions for atmospheric turbulence with zero-boresight pointing errors over deterministic as well as random path-loss in foggy conditions with heterodyne detection (HD) and intensity modulation/direct detection (IM/DD) methods. By deriving the probability density function (PDF) and cumulative distribution function (CDF) of the direct-link (DL) with the statistical effect of atmospheric turbulence, pointing errors and random fog, we develop exact expressions of PDF and CDF of the resultant channel for the RISE-FSO system. Using the derived statistical results, we present exact expressions of outage probability, average bit-error-rate (BER), ergodic capacity, and moments of signal-to-noise ratio (SNR) for both DL-FSO and RISE-FSO systems. We also develop an asymptotic analysis of the outage probability and average BER and derive the diversity order of the considered systems. We validate the analytical expressions using Monte-Carlo simulations and demonstrate the performance scaling of the FSO system with the number of RIS elements for various turbulence channels, detection techniques, and weather conditions.

Index Terms—Atmospheric turbulence, diversity order, free-space optical (FSO), Fox’s H-function, performance analysis, pointing errors, reconfigurable intelligent surface (RIS).

I. INTRODUCTION

Reconfigurable intelligent surface (RIS) is a promising technology to empower wireless systems by artificially controlling the characteristics of propagating signals in a desired direction [1]–[5]. Specifically, RISs are constructed by planar metasurfaces using a large number of reflection units adapted by integrated electronics to control the phase, amplitude and polarization of incident signals. The RIS is a promising alternative to active relaying techniques without requiring complex processing at the relay to improve the performance of wireless systems. Free-space optical (FSO) communication is a potential technology to cater high data rate transmission with license-free operation over a huge bandwidth in the optical spectrum [6]. Comparing with radio-frequency (RF), FSO systems are immune to the electromagnetic interference and

have been considered a cost-effective solution for terrestrial backhaul/fronthaul wireless applications for 5G and beyond 5G networks [7], [8].

The FSO link is subjected to various channel impairments such as atmospheric turbulence, pointing errors, and other weather conditions. The atmospheric turbulence is the scintillation effect of light propagation and introduces fading in the transmitted signal. In addition to the atmospheric turbulence, the range of FSO link is limited due to the higher signal attenuation, especially in the presence of fog and dust. Moreover, FSO is a line-of-sight (LOS) technology that may suffer significant performance degradation in the presence of pointing errors caused by the misalignment between the transmitter and the receiver. In this context, the deployment of FSO is not feasible for terrestrial applications due to the unavailability of a direct link in the presence of obstructions creating dead zones for wireless connectivity. The use of cooperative relaying has been extensively studied to mitigate the effect of channel impairments to improve the performance of FSO systems [9]–[12].

The advent of RIS opens an exciting research avenue to investigate and improve the performance of wireless systems for ubiquitous connectivity. Recently, the performance of RIS-enabled wireless systems have been analyzed over radio-frequency (RF) transmissions [13]–[22], mixed RF-FSO [23]–[25], and FSO systems [26]–[30]. In [23], a RIS-assisted dual-hop visible light communication (VLC)-RF system for an indoor scenario was proposed with VLC in the first link and RIS in the second RF link. In [24], the authors considered a decode-and-forward (DF) relaying to mix an FSO link over Gamma-Gamma turbulence with pointing errors and RF link assisted with RIS over Rayleigh fading. In a similar setup, the mixed RF-FSO system was analyzed in [25] by considering an additional co-channel interference (CCI) in the RF link. The use of relaying in such systems decouples the performance analysis for FSO and RF such that the impact of RIS is present only in the RF link without the challenges of analyzing the RIS for FSO transmissions with complicated fading models. Recently, the authors in [26]–[30] employ RIS module for FSO systems. An overview of various design aspects of optical RIS for FSO comparing with RIS-assisted RF is presented [26]. The authors in [27] characterized the impact of the physical parameters of the RIS to model the geometric and misalignment losses due to the random movements of the RIS and the effect of building sway. In [28], multiple optical RISs are used to improve the outage probability of the FSO system

Vinay Kumar Chapala (p20200110@pilani.bits-pilani.ac.in) and S. M. Zafaruddin (syed.zafaruddin@pilani.bits-pilani.ac.in) are with the Department of Electrical and Electronics Engineering, Birla Institute of Technology and Science, Pilani, Pilani-333031, Rajasthan, India.

This work was supported in part by the Science and Engineering Research Board (SERB), Department of Science and Technology (DST), Government of India, under Start-up Research Grant SRG/2019/002345.

under the effect of pointing errors without considering the atmospheric turbulence. The authors in [29], [30] considered the Gamma-Gamma atmospheric turbulence with pointing errors to analyze the RIS based FSO system. However, the authors in [30] considered a simplified model by considering a single-element RIS to assist the FSO system. Moreover, the authors in [29] used the Gaussian distribution to analyze the RIS-assisted FSO system by employing the central limit theorem to approximate the distribution function of the end-to-end channel. It is desirable to provide an exact analysis of the FSO system with atmospheric turbulence combined with pointing errors and assisted by the RIS with multiple elements. To this end, we emphasize that the RIS can be applied for both indoor and outdoor FSO communications. In indoor applications, when there is no direct link between the source and destination, the use of RIS (deployed on the ceiling or wall) can reflect the incident laser beam to the receiver coherently. In the devoid of RIS, the intensity of diffused light scattered from rough surfaces can be much lower for establishing the communication link [31]. The optical RIS module can also be mounted on the top of a building for outdoor applications, facilitating building to building (B2B) connection for high-speed backhaul links.

There are several statistical models in the literature to characterize the atmospheric turbulence depending on the severity of turbulence, type of wave propagation, and mathematical tractability of the model. The Gamma-Gamma (\mathcal{GG}) is widely accepted for moderate-to-strong turbulence regime [32], whereas the generalized Málaga model (\mathcal{M}) can be used for all irradiance conditions in homogeneous and isotropic turbulence [33]. Recently, the Fisher–Snedecor \mathcal{F} -distribution model for the atmospheric turbulence is proposed for its mathematical tractability [34]. On the other hand, the zero-boresight model proposed by [35] is widely used in the literature to characterize the pointing errors in FSO systems. Traditionally, signal attenuation for FSO transmissions is assumed to be deterministic and quantified using a visibility range, for example, less attenuation in haze and light fog and more loss of signal power in the dense fog [36]. However, recent measurement data confirm that the signal attenuation in the fog is not deterministic but follows a probabilistic model [37]. It should be noted that heterodyne detection (HD) and intensity modulation/direct detection (IM/DD) are the two main modes of detection in FSO systems. Considering such a diverse operation, it is desirable to unify the FSO using different models of atmospheric turbulence with pointing errors, path loss, and detection modes.

In this paper, we analyze the performance of a RIS-empowered FSO (RISE-FSO) system by unifying \mathcal{F} , \mathcal{GG} , and \mathcal{M} distributions for atmospheric turbulence with zero-boresight pointing errors over deterministic as well as random path-loss in foggy conditions with HD and IM/DD modes of detection. It is emphasized that such a unification is not straight forward and it is not available even for the direct-link (DL) FSO systems. The major contributions of the proposed work are summarized as follows:

- We derive the probability density function (PDF) and cumulative distribution function (CDF) of the combined statisti-

cal effect of random fog with atmospheric turbulence and pointing errors of a DL-FSO system by unifying \mathcal{F} , \mathcal{GG} , and \mathcal{M} atmospheric turbulence models such that the traditional deterministic path loss model remains a particular case for a unified performance analysis.

- To analyze the RISE-FSO, we derive exact closed form expressions of PDF and CDF for the resultant channel realized by the sum of products (SOP) of fading coefficients considered to be independent but not identically distributed (i.n.i.d) according to the DL-FSO fading channel.
- Using the derived PDF and CDF, we analyze the performance of RISE-FSO system by developing exact closed-form expressions of the outage probability, average bit-error-rate (BER), ergodic capacity, and moments of signal-to-noise ratio (SNR) in terms of Fox’s H-function. For comparison, we also develop an exact analysis of the aforementioned performance metrics for the DL-FSO system, which is not available under the combined effect of atmospheric turbulence, pointing errors, and random fog.
- We present asymptotic analysis for the outage probability and average BER in simpler Gamma function in the high SNR regime. The asymptotic expressions are readily tractable and provide engineering insights for system design. As such, we derive diversity order using the outage probability and average BER depicting the impact of atmospheric turbulence, pointing errors, and foggy channel on system behavior, and the scaling of FSO performance with an increase in the number of RIS elements.
- We validate the derived analytical results using extensive Monte-Carlo simulations demonstrating the effectiveness of RISE-FSO in comparison with the DL-FSO system for various atmospheric turbulence, detection techniques, and weather conditions.

A. Related Works

In this subsection, we summarize recent research works on RIS based RF systems. The authors in [13] analyzed outage probability, average bit-error-rate (BER) and bounds on capacity over Rayleigh fading RIS system. Considering the similar channel model, the authors in [14] presented the exact and asymptotic analysis of ergodic capacity. In [15], performance of RIS-assisted and amplify-and-forward (AF) relaying wireless systems were compared for Rayleigh fading channel where the RIS-assisted system was shown to outperform the corresponding relaying systems. In [16], for arbitrarily finite RIS elements, the authors offered closed-form estimates on the channel distribution over Rayleigh fading channels for dual-hop and transmit RIS-aided schemes. The authors used Rician fading to investigate the outage probability and ergodic capacity of a single-input single-output (SISO) RIS-assisted wireless communications system in [17]. The authors in [18], [19] approximated the average BER and ergodic capacity performance over Nakagami-m fading channels. Exact coverage analysis of RIS-enabled systems with Nakagami-m channels was presented in [20]. In [21], the authors derived exact expressions of the outage probability and ergodic capacity for a RIS-assisted system without pointing errors over generalized

Fox's H fading channels. In [38], the authors considered α - μ fading model and analyzed the effective rate of RIS-assisted communications by simplifying the analysis using the mixture of Gaussian instead of considering the sum of cascaded α - μ distributed random variables. In [22], the authors analyzed a RIS-assisted millimeter-wave communication over the fluctuating two rays (FTR) fading model in terms of Fox's H-function. Similarly, the authors in [39] extended the analysis for RIS-aided THz communications by deriving outage probability and ergodic capacity over FTR channel model combined with antenna misalignment and hardware impairments. Recently, the performance of RIS-assisted THz transmissions over α - μ fading channel with pointing errors is analyzed [40]. The research on RIS-assisted wireless systems is growing rapidly. To the best of authors' knowledge, exact performance analysis on RIS empowered FSO system over generalized atmospheric turbulence with pointing errors is not publicly available.

B. Notations and Organizations

Main notations used in this paper are summarized in Table I. The paper is organized as follows: system and channel models are summarized in Section II followed by statistical distribution functions of DL-FSO and RISE-FSO systems in Section III. Performance analysis through exact and asymptotic expressions is presented in Section IV. The numerical and simulation results are discussed in Section V. Finally, the paper concludes with Section VI.

II. SYSTEM MODEL

We consider a single-aperture FSO system where the source S wishes to communicate with the destination D . We assume that there is no direct link between the source and destination. To facilitate transmissions for the RISE-FSO, we employ an N -element optical RIS such that a LOS exists from source to the RIS and RIS to the destination, as shown in Fig. 1. Assuming perfect phase compensation at the RIS, the signal received at the destination through RIS is expressed as [29]

$$y = \sum_{i=1}^N h_i g_i s + \nu \quad (1)$$

where s is the transmitted signal with power P_T , h_i and g_i are channel fading coefficients between the source to the i -th RIS element and between the i -th RIS element to the destination, respectively, and ν is the additive Gaussian noise with variance σ_ν^2 . We denote by d the link distance between the source and destination, by d_1 the distance between the source and the RIS, and by d_2 the distance between the RIS and destination.

We consider that FSO links experience signal fading due to atmospheric turbulence, pointing errors, and foggy conditions such that the combined fading coefficient is denoted as $h_i = h_i^{(f)} h_i^{(t)} h_i^{(p)}$ and $g_i = g_i^{(f)} g_i^{(t)} g_i^{(p)}$, where superscripts (f) , (t) , and (p) denote the fog, atmospheric turbulence, and pointing errors, respectively. In what follows, we detail the modeling of the channel coefficient h_i . Note that we can model the channel coefficient g_i similar to h_i . However, we consider

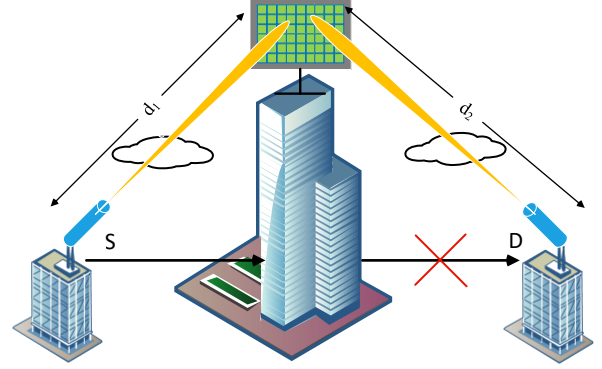


Fig. 1. Schematic diagram of RISE-FSO system for a typical outdoor application.

a general scenario considering fading coefficients h_i and g_i to be independent but non-identical distributed (i.n.i.d). Note that several publications employ the assumption of independent channels as a first approximation to analyze RIS-assisted systems [15], [16], [41], [42].

To characterize the statistics of pointing errors $h_i^{(p)}$, we use the recently proposed model for optical RIS in [28], which is based on the zero-boresight model [35]:

$$f_{h_i^{(p)}}(x) = \frac{\rho^2}{A_0 \rho^2} x^{\rho^2-1}, 0 \leq x \leq A_0, \quad (2)$$

where the term $A_0 = \text{erf}(v)^2$ denotes the fraction of collected power. Define $v = \sqrt{\pi/2} a_r / \omega_z$ with a_r as the aperture radius and ω_z as the beam width. We define the term $\rho^2 = \frac{\omega_{z_{\text{eq}}}^2}{\xi}$ where $\omega_{z_{\text{eq}}}$ is the equivalent beam-width at the receiver. The use of $\xi = 4\sigma_s^2$ models the DL-FSO, where σ_s^2 is the variance of pointing errors displacement characterized by the horizontal sway and elevation [35], while $\xi = 4\sigma_\theta^2 d^2 + 16\sigma_\beta^2 d_2^2$ models the pointing errors for the RIS-FSO system, where σ_θ and σ_β represent pointing error and RIS jitter angle standard deviation defined in [28]. It should be noted that the generalized non-zero boresight model [43], [44] can also be considered to model pointing errors for RIS-assisted FSO systems. Although it would be interesting to analyze the considered system with generalized pointing errors, we employ the zero-boresight model (as adopted in many reference papers) to avoid complicated analytical expressions. Further, the effect of non-zero boresight and unequal jitter is not significant on the performance of FSO systems [45].

For a unified performance analysis over a variety of turbulence conditions, we use the popular \mathcal{GG} [32], the generalized \mathcal{M} [33], and recently introduced \mathcal{F} -distribution [34] to model the atmospheric turbulence. We consider the \mathcal{M} -distribution since it is a generalized model applicable for a wide range of atmospheric turbulence from weak to super strong in the saturation regime for plane and spherical waves propagation. Further, \mathcal{GG} is the widely studied model applicable for moderate to strong turbulence conditions. Recently, the \mathcal{F} -distribution is proposed as a computationally efficient alternative to model

TABLE I
LIST OF MAIN NOTATIONS

Notation	Description	Notation	Description
$(\cdot)^{(f)}$	Fog	j	Imaginary number
$(\cdot)^{(t)}$	Atmospheric turbulence	$\mathbb{E}[\cdot]$	Expectation operator
$(\cdot)^{(p)}$	Pointing errors	$\exp(\cdot)$	Exponential function
$(\cdot)^{(tp)}$	Turbulence with pointing error	$(\cdot)^{(DL)}$	Direct link from source to destination
$G_{p,q}^{m,n} \left(x \left \begin{matrix} a \\ b \end{matrix} \right. \right)$	Meijer's G-function	$H_{p,q}^{m,n} \left(x \left \begin{matrix} (a, A) \\ (b, B) \end{matrix} \right. \right)$	Single-variate Fox's H-function
$\{a_i\}_1^N = \{a_1, \dots, a_N\}$	Shorthand notation	$\Gamma(a)$	$\int_0^\infty u^{a-1} e^{-u} du$

various atmospheric turbulence for spherical and Gaussian propagation scenarios. We denote by $h_i^{(tp)} = h_i^{(t)} h_i^{(p)}$ the combined effect of atmospheric turbulence and pointing errors. Note that the product distribution of atmospheric turbulence and pointing errors is available in the literature [10], [34], [46]. Thus, we represent the PDF of FSO link with \mathcal{GG} fading and pointing errors as given in [46]:

$$f_{h_i^{(tp)}}^{\text{GP}}(x) = \frac{\alpha_G \beta_G \rho^2}{A_0 \Gamma(\alpha_G) \Gamma(\beta_G)} G_{1,3}^{3,0} \left(\frac{\alpha_G \beta_G x}{A_0} \left| \begin{matrix} \rho^2 \\ \rho^2 - 1, \alpha_G - 1, \beta_G - 1 \end{matrix} \right. \right) \quad (3)$$

where the fading parameters α_G and β_G are defined in [32]. Similarly, the PDF of \mathcal{M} -distributed turbulence combined with pointing errors is given as [10]:

$$f_{h_i^{(tp)}}^{\text{MP}}(x) = \frac{\rho^2 A_{\text{mg}}}{2x} \sum_{m=1}^{\beta_M} b_m G_{1,3}^{3,0} \left(\frac{\alpha_M \beta_M x}{g \beta_M + \Omega'} \left| \begin{matrix} \rho^2 + 1 \\ \rho^2, \alpha_M, m \end{matrix} \right. \right) \quad (4)$$

where the parameters α_M , β_M , A_{mg} , b_m , and Ω' are given in [33]. Finally, the PDF of FSO channel experiencing \mathcal{F} -turbulence in the presence of pointing error impairments is given as [34]:

$$f_{h_i^{(tp)}}^{\text{FP}}(x) = \frac{\alpha_F \rho^2 G_{2,2}^{2,1} \left[\frac{\alpha_F}{(\beta_F - 1) A_0} x \left| \begin{matrix} -\beta_F, \rho^2 \\ \beta_F - 1, \rho^2 - 1 \end{matrix} \right. \right]}{(\beta_F - 1) A_0 \Gamma(\alpha_F) \Gamma(\beta_F)} \quad (5)$$

where the fading parameters α_F and β_F are listed in [47].

The channel coefficient $h_i^{(f)}$ models the path gain of signal transmission over the FSO link. Generally, $h_i^{(f)}$ is a deterministic quantity obtained from Beer-Lambert's Law $h_i^{(f)} = e^{-\tau d}$ where d is the link distance (in km) and τ is the atmospheric attenuation factor which depends on the wavelength and visibility range [36]. The atmospheric attenuation is defined as $\tau = \frac{3.19}{V} \left(\frac{\lambda}{550 \text{ nm}} \right)^{-q_v}$ where V is the visibility (in km), λ is operating wavelength (in nm), and q_v is the size distribution of the scattering particles as presented in [36]. However, recent studies [37], [48] show that the path gain in foggy conditions exhibit randomness modeled with the following PDF

$$f_{h_i^{(f)}}(x) = \frac{v^k}{\Gamma(k)} \left[\ln \left(\frac{1}{x} \right) \right]^{k-1} x^{v-1}, \quad (6)$$

where $0 < x \leq 1$, $v = 4.343/d\beta^{\text{fog}}$, $k > 0$ is the shape parameter, and $\beta^{\text{fog}} > 0$ is the scale parameter.

We also consider the DL-FSO system by considering the existence of a direct link between the source and destination as a means to compare with the RISE-FSO system:

$$y = h^{\text{DL}} s + \nu \quad (7)$$

where h^{DL} denotes the channel coefficient of the direct link. It should be noted that the performance of DL-FSO system with various atmospheric turbulence and pointing errors has been extensively studied in the literature. However, an exact analysis for the DL-FSO system with the effect of random fog is not available. In [49], we have developed asymptotic analysis by considering exponentiated Weibull model for atmospheric turbulence with pointing errors and random fog.

III. STATISTICAL RESULTS

In this section, we develop the PDF and CDF of the resultant channel $h = \sum_{i=1}^N h_i g_i$ of RISE-FSO system. First, we find density and distribution functions of the combined channel $h_i = h_i^{(f)} h_i^{(t)} h_i^{(p)}$ by unifying the PDF of various atmospheric turbulence with pointing errors as given in (3), (4), and (5). Next, we develop statistical results of $Z_i = h_i g_i$ using Mellin's transform. Finally, we use the MGF of Z_i to get the PDF and CDF of $Z = \sum_{i=1}^N Z_i$.

The PDF of the combined channel h_i can be computed as the product of PDFs of atmospheric turbulence $h^{(t)}$, pointing error $h^{(p)}$ and fog $h^{(f)}$. Since the PDF $h^{(tp)}$ (i.e., the product of atmospheric turbulence $h^{(t)}$, and pointing error $h^{(p)}$) is already available in the literature, we unify the PDF $h^{(tp)}$ given in (3), (4), and (5) for \mathcal{GG} , \mathcal{M} , and \mathcal{F} -distribution in the following Proposition 1, and use the unified distribution of $h^{(tp)}$ to derive the PDF of $h^{(tp)} h^{(f)}$ using the theory of product distribution [50] in Theorem 1.

Proposition 1. *A unified PDF for the combined effect of atmospheric turbulence and pointing errors is given as*

$$f_{h_i^{(tp)}}(x) = \psi x^{\phi-1} \sum_{l=1}^P \zeta_l G_{p,q}^{m,n} \left(C_l x \left| \begin{matrix} \{a_{l,w}\}_{w=1}^p \\ \{b_{l,w}\}_{w=1}^q \end{matrix} \right. \right) \quad (8)$$

where parameters in (8) define specific atmospheric turbulence model, as given in Table II.

Proof: We use (8) as a general fading model and derive the parameters of specific models using (3), (4), and (5), as depicted in Table II. ■

It is straightforward to use (8) and find the PDF of combined channel $h_i = h_i^{(tp)} h_i^{(f)}$ if the channel gain $h_i^{(f)}$ is considered

TABLE II
PARAMETERS OF THE UNIFIED PDF (PROPOSITION 1)

Turbulence Model	Unified parameters
\mathcal{GG}	$\psi = \frac{\alpha_G \beta_G \rho^2}{A_0 \Gamma(\alpha_G) \Gamma(\beta_G)}, \phi = 1, P = 1, \zeta_1 = 1, C_1 = \frac{\alpha_G \beta_G}{A_0},$ $\{m, n, p, q\} = \{3, 0, 1, 3\}, a = \{\rho^2\}, b = \{\rho^2 - 1, \alpha_G - 1, \beta_G - 1\}$
\mathcal{M}	$\psi = \frac{\rho^2 A_M}{2}, \phi = 0, P = \beta_M, \zeta_1 = b_l, C_1 = \frac{\alpha_M \beta_M}{(g \beta_M + \Omega) A_0},$ $\{m, n, p, q\} = \{3, 0, 1, 3\}, a = \{\rho^2 + 1\}, b = \{\rho^2, \alpha_M, l\}$
\mathcal{F}	$\psi = \frac{\alpha_F \rho^2}{(\beta_F - 1) h_1 A_0 \Gamma(\alpha_F) \Gamma(\beta_F)}, \phi = 1, P = 1, \zeta_1 = 1, C_1 = \frac{\alpha_F}{(\beta_F - 1) h_1 A_0},$ $\{m, n, p, q\} = \{2, 1, 2, 2\}, a = \{-\beta_F, \rho^2\}, b = \{\alpha_F - 1, \rho^2 - 1\}$

to be deterministic. In the following Theorem, we develop a novel PDF considering the channel gain $h_i^{(f)}$ to be distributed according to (6) in the presence of fog.

Theorem 1. *If k and v are the parameters of the foggy channel and Table II depicts the parameters for atmospheric turbulence and pointing errors, then the PDF and CDF of the combined fading channel with atmospheric turbulence, pointing errors, and random fog are given by*

$$f_{h_i}(x) = \psi v^k x^{\phi-1} \sum_{l=1}^P \zeta_l G_{p+k, q+k}^{m+k, n} \left[C_l x \left| \begin{array}{c} \{a_{l,w}\}_{w=1}^p, \{v - \phi + 1\}_1^k \\ \{b_{l,w}\}_{w=1}^m, \{v - \phi\}_1^k, \{b_{l,w}\}_{w=m+1}^q \end{array} \right. \right] \quad (9)$$

$$F_{h_i}(x) = \psi v^k x^\phi \sum_{l=1}^P \zeta_l G_{p+k+1, q+k+1}^{m+k, n+1} \left[C_l x \left| \begin{array}{c} \{a_{l,w}\}_{w=1}^n, \{1 - \phi\}, \{a_{l,w}\}_{w=n+1}^p, \{v - \phi + 1\}_1^k \\ \{b_{l,w}\}_{w=1}^m, \{v - \phi\}_1^k, \{b_{l,w}\}_{w=m+1}^q, \{-\phi\} \end{array} \right. \right] \quad (10)$$

Proof: See Appendix A. ■

Note that the parameter k should be a positive integer to satisfy the definition of Meijer's G-function. Since the underlying PDFs in (8) and (9) have a similar structure, the unified performance analysis presented in this paper is applicable for both deterministic and random path loss model. As such, the PDF represented in (9) can be reduced to (8) for the deterministic path gain by substituting $k = 0$ and limiting the argument of Meijer's G-function up to p and q terms.

To facilitate performance analysis for the RISE-FSO, the distribution function of $\sum_{i=1}^N h_i g_i$ is required. Considering L reflecting paths in each RIS element, we derive the PDF and CDF of the generalized system $Z = \sum_{i=1}^N Z_i$, where $Z_i = \prod_{j=1}^L h_{i,j}$ and $h_{i,j}, j = 1, 2, \dots, L$ are i.n.i.d random variable distributed according to (9). Note that we can use the results of Theorem 1 to analyze the performance of the DL-FSO system.

Proposition 2. *If k and v are the parameters of the foggy channel and Table II depicts the parameters for atmospheric turbulence and pointing errors, then the PDF and CDF, and MGF of a product of L independent but non-identical (i.n.i.d) random variables $Z_i = \prod_{j=1}^L h_{i,j}$ are given by*

$$f_{Z_i}(x) = \frac{1}{x} \sum_{l_1, \dots, l_L=1}^P \prod_{j=1}^L \psi_j v_j^{k_j} \zeta_{l_j} \left(C_{l_j} \right)^{-\phi_j} G_{pL + \sum_{j=1}^L k_j, qL + \sum_{j=1}^L k_j}^{mL + \sum_{j=1}^L k_j, nL} \left[x \prod_{j=1}^L C_{l_j} \left| \begin{array}{c} V_1, V_2 \\ V_3 \end{array} \right. \right] \quad (11)$$

$$F_{Z_i}(x) = \sum_{l_1, \dots, l_L=1}^P \prod_{j=1}^L \psi_j v_j^{k_j} \zeta_{l_j} \left(C_{l_j} \right)^{-\phi_j} G_{pL + \sum_{j=1}^L k_j, nL+1}^{mL + \sum_{j=1}^L k_j + 1, qL + \sum_{j=1}^L k_j + 1} \left[x \prod_{j=1}^L C_{l_j} \left| \begin{array}{c} V_1, \{1\}, V_2 \\ V_3, \{0\} \end{array} \right. \right] \quad (12)$$

$$M_{Z_i}(s) = \sum_{l_1, \dots, l_L=1}^P \prod_{j=1}^L \psi_j v_j^{k_j} \zeta_{l_j} \left(C_{l_j} \right)^{-\phi_j} G_{pL + \sum_{j=2}^L k_j + 1, qL + \sum_{j=1}^L k_j}^{mL + \sum_{j=1}^L k_j, nL+1} \left[\frac{1}{s} \prod_{j=1}^L C_{l_j} \left| \begin{array}{c} V_1, \{1\}, V_2 \\ V_3 \end{array} \right. \right] \quad (13)$$

where $V_1 = \{\{\phi_j + a_{l_j, w}\}_{w=1}^L\}_{w=1}^n$, $V_2 = \{\{\phi_j + a_{l_j, w}\}_{w=1}^L\}_{w=n+1}^p, \{\{v_j + 1\}_1^{k_j}\}_{j=1}^L$ and $V_3 = \{\{\phi_j + b_{l_j, w}\}_{w=1}^L\}_{w=1}^m, \{\{v_j\}_1^{k_j}\}_{j=1}^L, \{\{\phi_j + b_{l_j, w}\}_{w=1}^L\}_{w=m+1}^q$.

Proof: See Appendix B. ■

Theorem 2. *If k and v are the parameters of the foggy channel and Table II depicts the parameters for atmospheric turbulence and pointing errors, then the PDF and CDF of $Z = \sum_{i=1}^N Z_i$ are given by (14) and (15) respectively.*

Proof: See Appendix C. ■

As a special case to simplify the notation of multi-variate Fox's H-function, we use $L = 2$ in (14) (which corresponds to the system model, as shown in Fig. 1) with $N = 2$ RIS elements and similar foggy conditions depicted by $k_{i,j} = k \forall i, j$ to express the PDF (14) in terms of simpler Bi-variate Fox's H-function:

$$f_Z(x) = \frac{1}{x} \sum_{l_1, l_2=1}^P \sum_{l_1, l_2=1}^P \prod_{i=1}^2 \prod_{j=1}^2 \psi_{i,j} v_{i,j}^{k_{i,j}} \zeta_{l_{i,j}} \left(C_{l_{i,j}} \right)^{-\phi_{i,j}} H_{0,0:2m+2k, 2n+1; 2m+2k, 2n+1}^{0,1:2p+2k+1, 2q+2k; 2p+2k+1, 2q+2k} \left[x \prod_{j=1}^2 C_{l_{1,j}} \left| \begin{array}{c} - : V_1 \\ (1, 1, \dots, 1) : V_2 \end{array} \right. \right] \quad (16)$$

where $V_1 = \{\{\{\phi_{i,j} + a_{l_{i,j}, w}\}_{w=1}^2\}_{j=1}^n, (1, 1), \{\{\phi_{i,j} + a_{l_{i,j}, w}\}_{w=1}^2\}_{j=1}^p, \{\{(v_{i,j} + 1)\}_1^{k_{i,j}}\}_{j=1}^2\}_{i=1}^2$ and $V_2 = \{\{\{\phi_{i,j} + b_{l_{i,j}, w}\}_{w=1}^2\}_{j=1}^m, \{\{(v_{i,j}, 1)\}_1^{k_{i,j}}\}_{j=1}^2, \{\{\phi_{i,j} + b_{l_{i,j}, w}\}_{w=1}^2\}_{j=1}^q, \{1\}_{i=1}^2\}_{i=1}^2$.

Similarly, we can simplify the CDF in (15) for $L = 2$, $N = 2$, and $k_{i,j} = k \forall i, j$. In what follows, we analyze the

$$f_Z(x) = \frac{1}{x} \sum_{l_{1,1}, \dots, l_{1,L}=1}^P \cdots \sum_{l_{N,1}, \dots, l_{N,L}=1}^P \prod_{i=1}^N \prod_{j=1}^L \psi_{i,j} v_{i,j}^{k_{i,j}} \zeta_{i,j} \left(C_{l_{i,j}} \right)^{-\phi_{i,j}}$$

$$H_{0,0; 0,1; pL+\sum_{j=1}^L k_{1,j}+1, qL+\sum_{j=1}^L k_{1,j}; \dots; mL+\sum_{j=1}^L k_{N,j}, nL+1} \left[\begin{array}{c} x \prod_{j=1}^L C_{l_{i,j}} \\ \vdots \\ x \prod_{j=1}^L C_{l_{i,j}} \end{array} \middle| \begin{array}{l} - : V_1 \\ (1; 1, \dots, 1) : V_2 \end{array} \right] \quad (14)$$

$$F_Z(x) = \sum_{l_{1,1}, \dots, l_{1,L}=1}^P \cdots \sum_{l_{N,1}, \dots, l_{N,L}=1}^P \prod_{i=1}^N \prod_{j=1}^L \psi_{i,j} v_{i,j}^{k_{i,j}} \zeta_{i,j} \left(C_{l_{i,j}} \right)^{-\phi_{i,j}}$$

$$H_{0,0; 0,1; pL+\sum_{j=1}^L k_{1,j}+1, qL+\sum_{j=1}^L k_{1,j}; \dots; mL+\sum_{j=1}^L k_{N,j}, nL+1} \left[\begin{array}{c} x \prod_{j=1}^L C_{l_{i,j}} \\ \vdots \\ x \prod_{j=1}^L C_{l_{i,j}} \end{array} \middle| \begin{array}{l} - : V_1 \\ (0; 1, \dots, 1) : V_2 \end{array} \right] \quad (15)$$

where $V_1 = \{ \{ \{ (\phi_{i,j} + a_{l_{i,j},w}, 1) \}_{j=1}^L \}_{w=1}^n, (1, 1), \{ \{ (\phi_{i,j} + a_{l_{i,j},w}, 1) \}_{j=1}^L \}_{w=n+1}^p, \{ \{ (v_{i,j} + 1, 1) \}_1^{k_{i,j}} \}_{j=1}^L \}_{i=1}^N$ and $V_2 = \{ \{ \{ (\phi_{i,j} + b_{l_{i,j},w}, 1) \}_{j=1}^L \}_{w=1}^m, \{ \{ (v_{i,j}, 1) \}_1^{k_{i,j}} \}_{j=1}^L, \{ \{ (\phi_{i,j} + b_{l_{i,j},w}, 1) \}_{j=1}^L \}_{w=m+1}^q \}_{i=1}^N$.

performance of RISE-FSO and DL-FSO systems using the statistical results of Theorem 1 and Theorem 2, respectively.

IV. PERFORMANCE ANALYSIS

In this section, we analyze the performance of the RISE-FSO by a simple customization of Theorem 2 with $L = 2$, $z_{i,1} = h_i$, and $z_{i,2} = g_i$, which corresponds to the RISE-FSO system model in (1). Thus, we denote the resultant by $h = \sum_{i=1}^N h_i g_i$. Finally, we introduce the third unification of performance evaluation with HD ($t = 1$) and IM/DD ($t = 2$) detection modes by defining the SNR of the system as $\gamma = \gamma_0 h^t$, where $\gamma_0 = \frac{P_s^t}{\sigma_s^2}$. Using a straightforward transformation of the random variable, the CDF of SNR $F_\gamma(\gamma) = \Pr(\gamma_0 h^t \leq \gamma) = \Pr(h \leq (\frac{\gamma}{\gamma_0})^{1/t}) = F_h((\frac{\gamma}{\gamma_0})^{1/t})$ is given by

$$F_\gamma(\gamma) = F_h \left(\left(\frac{\gamma}{\gamma_0} \right)^{1/t} \right) \quad (17)$$

where $F_h(\cdot)$ is given in (15) with $L = 2$. Using (17), the PDF of SNR can be expressed as

$$f_\gamma(\gamma) = \frac{1}{t \gamma_0^{1/t} \gamma^{1-1/t}} f_h \left(\left(\frac{\gamma}{\gamma_0} \right)^{1/t} \right) \quad (18)$$

where $f_h(\cdot)$ is given in (14) with $L = 2$. Similarly, we use (9) and (10) to express the PDF and CDF of SNR for the DL-FSO as

$$f_\gamma^{\text{DL}}(\gamma) = \frac{1}{t \gamma_0^{1/t} \gamma^{1-1/t}} f_{h_i} \left(\left(\frac{\gamma}{\gamma_0} \right)^{1/t} \right),$$

$$F_\gamma^{\text{DL}}(\gamma) = F_{h_i} \left(\left(\frac{\gamma}{\gamma_0} \right)^{1/t} \right) \quad (19)$$

Using $t = 1$ and $t = 2$ in (19), the PDF and CDF of the SNR for HD and IM/DD detection techniques can be verified for the \mathcal{GG} turbulence (see [51] and references therein).

A. Outage Probability

Outage probability is a performance metric to characterize the impact of fading in a communication system. Mathematically, it can be defined as the probability of SNR falling below a threshold value γ_{th} i.e., $P_{\text{out}} = \Pr(\gamma \leq \gamma_{\text{th}})$.

Lemma 1. *We present the following results of outage probability for the RISE-FSO system:*

- An exact expression for the outage probability is given as $P_{\text{out}} = F_\gamma(\gamma_{\text{th}})$.
- Asymptotically at a high SNR, the outage probability is given by (20).
- The diversity order is given as $G_{\text{out}} = \sum_{i=1}^N \min \{ \{ \frac{\phi_{i,1} + b_{l_{i,1},w}}{t} \}_{w=1}^m, \frac{v_{i,1}}{t}, \{ \frac{\phi_{i,2} + b_{l_{i,2},w}}{t} \}_{w=1}^m, \frac{v_{i,2}}{t} \}$.

Proof: Part (a) can be obtained using the direct definition of the outage probability. To prove part (b), we use [52, Eqn. (30)] to derive the outage probability asymptotically at a high SNR $\gamma_0 \rightarrow \infty$ in terms of Gamma function. As such, the asymptotic expression in (20) is obtained by computing the residue of multiple Mellin-Barnes integrals of the corresponding multi-variate Fox's H-function at the dominant pole $p_i = \min \{ \{ \phi_{i,j} + b_{l_{i,j},w} \}_{w=1}^m, v_{i,j} \}_{j=1}^2$. To prove (c), we need to express (20) as $P_{\text{out}}^\infty \propto \gamma_0^{-G_{\text{out}}}$ in order to get the outage-diversity order G_{out} of the system. Using the dominant pole $p_i, \forall l_{i,j}, j$ (i.e., considering over all the summation terms in (20)), the N -products of the term $\gamma_0^{-\frac{p_i}{t}}$ result into $P_{\text{out}}^\infty \propto \gamma_0^{-\sum_{i=1}^N \frac{p_i}{t}}$. Finally, we use p_i to get the diversity order G_{out} as given in part (c). ■

We present Table III with $\kappa = 0$ for the diversity order of RISE-FSO system for three turbulence models and both the HD and IM/DD detection modes. It can be seen that the outage performance of the RISE-FSO improves with an increase in the number of RIS elements.

$$P_{\text{out}}^{\infty} \approx \sum_{l_{1,1}, l_{1,2}=1}^P \cdots \sum_{l_{N,1}, l_{N,2}=1}^P \prod_{i=1}^N \prod_{j=1}^2 \psi_{i,j} v_{i,j}^{k_{i,j}} \zeta_{i,j} (C_{l_{i,j}})^{-\phi_{i,j}} \left(\frac{\gamma_{\text{th}}}{\gamma_0}\right)^{p_i/t} \left(\prod_{j=1}^2 C_{l_{i,j}}\right)^{p_i} \frac{1}{\Gamma(1 + \sum_{i=1}^N p_i)}$$

$$\prod_{i=1}^N \frac{\prod_{j=1}^2 \prod_{w=1, p_i \neq \phi_{i,j} + b_{l_{i,j},w}}^m \Gamma(\phi_{i,j} + b_{l_{i,j},w} - p_i) \prod_{j=1, p_i \neq v_{i,j}}^2 (\Gamma(v_{i,j} - p_i))^{k_{i,j}} \prod_{j=1}^2 \prod_{w=1}^n \Gamma(1 - \phi_{i,j} - a_{l_{i,j},w} + p_i) \Gamma(p_i)}{\prod_{j=1}^2 \prod_{w=n+1}^p \Gamma(\phi_{i,j} + a_{l_{i,j},w} - p_i) \prod_{j=1}^2 (\Gamma(v_{i,j} + 1 - p_i))^{k_{i,j}} \prod_{j=1}^2 \prod_{w=m+1}^q \Gamma(1 - \phi_{i,j} - b_{l_{i,j},w} + p_i)} \quad (20)$$

where $p_i = \min\{\{\phi_{i,j} + b_{l_{i,j},w}\}_{w=1}^m, v_{i,j}\}_{j=1}^2$.

$$P_{\text{out}}^{\infty, \text{DL}} \approx \psi v^k \sum_{l=1}^P \zeta_l C_l^{-\phi} \left[\sum_{i=1}^m \frac{\prod_{w=1, w \neq i}^m \Gamma(b_{l,w} - b_{l,i}) (\Gamma(v - \phi - b_{l,i}))^k \prod_{w=1}^n \Gamma(1 - a_{l,w} + b_{l,i}) \Gamma(\phi + b_{l,i})}{\prod_{w=n+1}^p \Gamma(a_{l,w} - b_{l,i}) (\Gamma(v + 1 - \phi - b_{l,i}))^k \prod_{w=m+1}^q \Gamma(1 - b_{l,w} + b_{l,i}) \Gamma(1 + \phi + b_{l,i})} \right. \\ \left. \left(C_l^{\phi + b_{l,i}} \left(\frac{\gamma_{\text{th}}}{\gamma_0}\right)^{(\phi + b_{l,i})/t} \right) + k \frac{\prod_{w=1}^m \Gamma(\phi + b_{l,w} - v) \prod_{w=1}^n \Gamma(1 - \phi - a_{l,w} + v) \Gamma(v)}{\prod_{w=n+1}^p \Gamma(\phi + a_{l,w} - v) \prod_{w=m+1}^q \Gamma(1 - \phi - b_{l,w} + v) \Gamma(1 + v)} \left(C_l^v \left(\frac{\gamma_{\text{th}}}{\gamma_0}\right)^{v/t} \right) \right] \quad (21)$$

For the DL-FSO system, an exact expression of the outage probability can be obtained using the CDF in (19) and (10) as $P_{\text{out}}^{\text{DL}} = F_{\gamma}^{\text{DL}}(\gamma_{\text{th}})$. We use the asymptotic representation of the Meijer's G-function [53, 07.34.06.0005.01] on the derived $P_{\text{out}}^{\text{DL}}$ to express the outage probability in the high SNR regime $\gamma_0 \rightarrow \infty$, as (21).

To derive the diversity order of the DL-FSO system, we require the dominant term of $\gamma_0^{-(\phi + b_{l,i})/t}$ and $\gamma_0^{-(v)/t}$ over P and m summation terms in (21). Thus, we express $P_{\text{out}}^{\infty, \text{DL}} \propto \gamma_0^{-G_{\text{out}}^{\text{DL}}}$ using the minimum exponent of γ_0 to get $G_{\text{out}}^{\text{DL}} = \min\{\{\frac{\phi + b_{l,i}}{t}\}_{l=1, i=1}^P, \frac{v}{t}\}$. Using Table II, the diversity order for \mathcal{F} , \mathcal{GG} , and \mathcal{M} turbulence with pointing errors and random fog parameters are respectively, $\min\{\frac{\alpha_{\mathcal{F}}}{t}, \frac{\rho_{\mathcal{F}}^2}{t}, \frac{v}{t}\}$, $\min\{\frac{\rho_{\mathcal{G}}^2}{t}, \frac{\alpha_{\mathcal{G}}}{t}, \frac{\beta_{\mathcal{G}}}{t}, \frac{v}{t}\}$, and $\min\{\frac{\rho_{\mathcal{M}}^2}{t}, \frac{\alpha_{\mathcal{M}}}{t}, \frac{\beta_{\mathcal{M}}}{t}, \frac{v}{t}\}$. This is consistent with previous results of diversity order for DL-FSO systems with atmospheric turbulence and pointing errors with deterministic path loss (see [10] [11] [47], and references therein).

B. Average BER

Average BER is used to quantify the reliability of data transmissions. For binary modulations, the average BER using the CDF of SNR is given as [54]

$$\bar{P}_e = \frac{q^p}{2\Gamma(p)} \int_0^{\infty} \gamma^{p-1} e^{-q\gamma} F_{\gamma}(\gamma) d\gamma \quad (22)$$

where p and q are modulation specific parameters. Specifically, for coherent binary FSK (CBFSK), $p = q = 0.5$, coherent binary PSK (CBPSK), $p = 0.5$ and $q = 1$, non-coherent binary FSK (NBFSK), $p = 1$ and $q = 0.5$, differential binary PSK (DBPSK), $p = 1$ and $q = 1$.

Lemma 2. We present the following results of the average BER for the RISE-FSO system:

- An exact expression for the average BER is given by (23).
- Asymptotically at high SNR $\gamma_0 \rightarrow \infty$, the average BER can be expressed as (24).
- The diversity order using the average BER is $G_{\text{BER}} = \sum_{i=1}^N \min\{\{\frac{\phi_{i,j} + b_{l_{i,j},w} - 1}{t}\}_{w=1}^m, \frac{v_{i,j} - 1}{t}\}_{j=1}^2$.

Proof: To prove (a), we substitute the CDF of the RISE-FSO system of (17) (which requires (15)) in (22), use the definition of multivariate Fox's H-function and interchange the order of integration to get

$$\bar{P}_e = \frac{q^p}{2\Gamma(p)} \sum_{l_{1,1}, l_{1,2}=1}^P \cdots \sum_{l_{N,1}, l_{N,2}=1}^P \prod_{j=1}^N \prod_{j=1}^2 \psi_{i,j} v_{i,j}^{k_{i,j}} \zeta_{i,j} \\ (C_{l_{i,j}})^{-\phi_{i,j}} \left(\left(\frac{1}{2\pi j}\right)^N \int_{\mathcal{L}_i} \left(\left(\frac{1}{\gamma_0}\right)^{1/t} \prod_{j=1}^2 C_{l_{i,j}}\right)^{x_i} \right. \\ \left. \left[\frac{\prod_{j=1}^2 \prod_{w=1}^m \Gamma(-x_i + \phi_{i,j} + b_{l_{i,j},w})}{\prod_{j=1}^2 \prod_{w=n+1}^p \Gamma(-x_i + \phi_{i,j} + a_{l_{i,j},w})} \frac{\prod_{j=1}^2 \prod_{w=1}^n \Gamma(1 + x_i - \phi_{i,j} - a_{l_{i,j},w})}{\prod_{j=1}^2 \prod_{w=m+1}^q \Gamma(1 + x_i - \phi_{i,j} - b_{l_{i,j},w})} \frac{\prod_{j=1}^2 (\Gamma(v_{i,j} - x_i))^{k_{i,j}}}{\prod_{j=1}^2 (\Gamma(1 + v_{i,j} - x_i))^{k_{i,j}}} \right. \right. \\ \left. \left. \frac{\Gamma(x_i)}{\Gamma(1 + \sum_{i=1}^N x_i)} \right] \left(\int_0^{\infty} e^{-q\gamma} \gamma^{p-1} \gamma^{\frac{1}{t} \sum_{i=1}^N x_i} d\gamma \right) dx_i \right) \quad (25)$$

We solve the inner integral in (25):

$$\int_0^{\infty} e^{-q\gamma} (\gamma)^{p-1 + \frac{1}{t} \sum_{i=1}^N x_i} d\gamma = \left(\frac{1}{q}\right)^{p + \frac{1}{t} \sum_{i=1}^N x_i} \Gamma\left(p + \frac{1}{t} \sum_{i=1}^N x_i\right) \quad (26)$$

Using (26) in (25), we apply the definition of N -multivariate Fox's H-function [55, A.1] to get (23). To prove (b), we use the asymptotic analysis in [52, (31)] to express the average BER at a high SNR in (24). To prove (c), we express $\bar{P}_e^{\infty} \propto \gamma_0^{-G_{\text{BER}}}$ using the similar procedure as depicted in deriving the outage-diversity order (see proof of Lemma 1, part (c)). ■

Similar to the outage probability, we list the diversity order of the RISE-FSO system using the average BER in Table III with $\kappa = 1$. The diversity order shows that the performance of the RISE FSO system improves with an increase in the number of RIS elements.

The average BER of the DL-FSO system can be derived using (10) in (22) and applying the similar procedure used in RISE-FSO with the inner integral $\int_0^{\infty} e^{-q\gamma} \gamma^{p-1} \gamma^{x/t} d\gamma = \frac{1}{q^{p+\frac{x}{t}}} \Gamma\left(p + \frac{x}{t}\right)$ to get (27). We use the asymptotic analysis of univariate Fox's H-function provided in [56] to express average BER of the DL-FSO at a high SNR as (28).

To derive the BER-diversity order of the DL-FSO system, we express $\bar{P}_e^{\infty, \text{DL}} \propto \gamma_0^{-G_{\text{BER}}^{\text{DL}}}$ using the minimum exponent of $\gamma_0^{-(\phi + b_{l,i})/t}$ and $\gamma_0^{-(v)/t}$ over P and m summation terms

TABLE III
DIVERSITY ORDER OF RISE-FSO

Turbulence Model	G_{out} with $\kappa = 0$ and G_{BER} with $\kappa = 1$
\mathcal{GG}	$\sum_{i=1}^N \min\left\{\frac{\alpha_G(i,1)-\kappa}{t}, \frac{\beta_G(i,1)-\kappa}{t}, \frac{\rho_{i,1}^2-\kappa}{t}, \frac{v_{i,1}-\kappa}{t}, \frac{\alpha_G(i,2)-\kappa}{t}, \frac{\beta_G(i,2)-\kappa}{t}, \frac{\rho_{i,2}^2-\kappa}{t}, \frac{v_{i,2}-\kappa}{t}\right\}$
\mathcal{M}	$\sum_{i=1}^N \min\left\{\frac{\alpha_M(i,1)-\kappa}{t}, \frac{\beta_M(i,1)-\kappa}{t}, \frac{\rho_{i,1}^2-\kappa}{t}, \frac{v_{i,1}-\kappa}{t}, \frac{\alpha_M(i,2)-\kappa}{t}, \frac{\beta_M(i,2)-\kappa}{t}, \frac{\rho_{i,2}^2-\kappa}{t}, \frac{v_{i,2}-\kappa}{t}\right\}$
\mathcal{F}	$\sum_{i=1}^N \min\left\{\frac{\alpha_F(i,1)-\kappa}{t}, \frac{\rho_{i,1}^2-\kappa}{t}, \frac{v_{i,1}-\kappa}{t}, \frac{\alpha_F(i,2)-\kappa}{t}, \frac{\rho_{i,2}^2-\kappa}{t}, \frac{v_{i,2}-\kappa}{t}\right\}$

$$\bar{P}_e = \left(\frac{1}{2\Gamma(p)}\right) \sum_{l_{1,1}, l_{1,2}=1}^P \cdots \sum_{l_{N,1}, l_{N,2}=1}^P \prod_{i=1}^N \prod_{j=1}^2 \psi_{i,j} v_{i,j}^{k_{i,j}} \zeta_{l_{i,j}} \left(C_{l_{i,j}}\right)^{-\phi_{i,j}}$$

$$H_{1,1:2m+k_{1,1}+k_{1,2}, 2n+1; \dots; 2m+k_{N,1}+k_{N,2}, 2n+1}^{0,1} \left[\begin{array}{c} \left(\frac{1}{q\gamma_0}\right)^{1/t} \prod_{j=1}^2 C_{l_{i,j}} \\ \vdots \\ \left(\frac{1}{q\gamma_0}\right)^{1/t} \prod_{j=1}^2 C_{l_{i,j}} \end{array} \middle| \begin{array}{c} (1-p, \frac{1}{t}, \dots, \frac{1}{t}) : V_1 \\ (0; 1, \dots, 1) : V_2 \end{array} \right] \quad (23)$$

where $V_1 = \{(\phi_{i,1} + a_{l_{i,1},w}, 1)\}_{w=1}^n, (\phi_{i,2} + a_{l_{i,2},w}, 1)\}_{w=1}^n, (1, 1), \{(\phi_{i,1} + a_{l_{i,1},w}, 1)\}_{w=n+1}^p, \{(\phi_{i,2} + a_{l_{i,2},w}, 1)\}_{w=n+1}^p, \{(v_{i,1} + 1, 1)\}_1^{k_{i,1}}, \{(v_{i,2} + 1, 1)\}_1^{k_{i,2}}\}_{i=1}^N$ and $V_2 = \{(\phi_{i,1} + b_{l_{i,2},w}, 1)\}_{w=1}^m, \{(\phi_{i,2} + b_{l_{i,2},w}, 1)\}_{w=1}^m, \{(v_{i,1}, 1)\}_1^{k_{i,1}}, \{(v_{i,2}, 1)\}_1^{k_{i,2}}, \{(\phi_{i,1} + b_{l_{i,1},w}, 1)\}_{w=m+1}^q, \{(\phi_{i,2} + b_{l_{i,2},w}, 1)\}_{w=m+1}^q\}_{i=1}^N$.

$$\bar{P}_e^\infty \approx \sum_{l_{1,1}, l_{1,2}=1}^P \cdots \sum_{l_{N,1}, l_{N,2}=1}^P \prod_{i=1}^N \prod_{j=1}^2 \frac{\psi_{i,j} v_{i,j}^{k_{i,j}}}{2\Gamma(p)} \zeta_{l_{i,j}} (C_{l_{i,j}})^{N+p_i-1-\phi_{i,j}} \left(\frac{1}{q\gamma_0}\right)^{\frac{p_i-1}{t}} \left(\frac{1}{q}\right)^{N/t} \frac{\Gamma(p + \frac{1}{t} \sum_{i=1}^N p_i)}{\Gamma(1 + \sum_{i=1}^N p_i)}$$

$$\prod_{i=1}^N \frac{\prod_{j=1}^2 \prod_{w=1, p_i \neq \phi_{i,j} + b_{l_{i,j},w}}^m \Gamma(\phi_{i,j} + b_{l_{i,j},w} - p_i) \prod_{j=1, p_i \neq v_{i,j}}^2 (\Gamma(v_{i,j} - p_i))^{k_{i,j}} \prod_{j=1}^2 \prod_{w=1}^n \Gamma(1 - \phi_{i,j} - a_{l_{i,j},w} + p_i) \Gamma(p_i)}{\prod_{j=1}^2 \prod_{w=n+1}^p \Gamma(\phi_{i,j} + a_{l_{i,j},w} - p_i) \prod_{j=1}^2 (\Gamma(v_{i,j} + 1 - p_i))^{k_{i,j}} \prod_{j=1}^2 \prod_{w=m+1}^q \Gamma(1 - \phi_{i,j} - b_{l_{i,j},w} + p_i)} \quad (24)$$

where $p_i = \min\{\{\phi_{i,1} + b_{l_{i,1},w}\}_{w=1}^m, v_{i,1}, \{\phi_{i,2} + b_{l_{i,2},w}\}_{w=1}^m, v_{i,2}\}$.

$$\bar{P}_e^{\text{DL}} = \frac{\psi v^k}{2\Gamma(p)} \sum_{l=1}^P \zeta_l C_l^{-\phi} H_{p+k+2, q+k+1}^{m+k, n+2} \left[C_l \left(\frac{1}{q\gamma_0}\right)^{1/t} \middle| \begin{array}{c} \{(\phi + a_{l,w}, 1)\}_{w=1}^n, (1, 1), (1-p, \frac{1}{t}), \{(\phi + a_{l,w}, 1)\}_{w=n+1}^p, \{(v+1, 1)\}_1^k \\ \{(\phi + b_{l,w}, 1)\}_{w=1}^m, \{(v, 1)\}_1^k, \{(\phi + b_{l,w}, 1)\}_{w=m+1}^q, (0, 1) \end{array} \right] \quad (27)$$

in (28) to get $G_{\text{BER}}^{\text{DL}} = \min(\{\frac{\phi+b_{l,i}}{t}\}_{l=1, i=1}^{l=P, i=m}, \frac{v}{t})$. Hence, the diversity order of the DL-FSO system for \mathcal{F} , \mathcal{GG} , and \mathcal{M} are given, respectively as $\min\{\frac{\alpha_F}{t}, \frac{\rho^2}{t}, \frac{v}{t}\}$, $\min\{\frac{\rho^2}{t}, \frac{\alpha_G}{t}, \frac{\beta_G}{t}, \frac{v}{t}\}$, and $\min\{\frac{\rho^2}{t}, \frac{\alpha_M}{t}, \frac{\beta_M}{t}, \frac{v}{t}\}$.

C. Ergodic Capacity

Assuming a Gaussian codebook at the channel input, the ergodic capacity of an FSO system defined as the maximum information transmission rate with an arbitrarily low error probability is given as [6]:

$$\bar{\eta} = \mathbb{E}[\log_2(1 + \mu_t \gamma)] = \int_0^\infty \log_2(1 + \mu_t \gamma) f_\gamma(\gamma) d\gamma \quad (29)$$

where $t \in \{1, 2\}$ with $\mu_1 = 1$ HD and $\mu_2 = \frac{e}{2\pi}$ for IM/DD receivers.

Lemma 3. *The ergodic capacity of the RISE-FSO is given by (30).*

Proof: We substitute the PDF of SNR of RISE-FSO system (18) through (14) in (29), use the definition of multivariate Fox's H-function, and change the order of integration to get

$$\bar{\eta} = \frac{\log_2(e)}{t} \sum_{l_{1,1}, l_{1,2}=1}^P \cdots \sum_{l_{N,1}, l_{N,2}=1}^P \prod_{i=1}^N \prod_{j=1}^2 \psi_{i,j} v_{i,j}^{k_{i,j}} \zeta_{l_{i,j}} (C_{l_{i,j}})^{-\phi_{i,j}} \left(\left(\frac{1}{2\pi j}\right)^N \int_{\mathcal{L}_i} \left(\left(\frac{1}{\gamma_0}\right)^{1/t} \prod_{j=1}^2 C_{l_{i,j}}\right)^{n_i} \right. \\ \left. \frac{\prod_{j=1}^2 \prod_{w=1}^m \Gamma(-x_i + \phi_{i,j} + b_{l_{i,j},w})}{\prod_{j=1}^2 \prod_{w=n+1}^p \Gamma(-x_i + \phi_{i,j} + a_{l_{i,j},w})} \frac{\prod_{j=1}^2 \prod_{w=1}^n \Gamma(1+x_i - \phi_{i,j} - a_{l_{i,j},w})}{\prod_{j=1}^2 \prod_{w=m+1}^q \Gamma(1+x_i - \phi_{i,j} - b_{l_{i,j},w})} \prod_{j=1}^2 (\Gamma(v_{i,j} - x_i))^{k_{i,j}} \right. \\ \left. \frac{\Gamma(x_i)}{\Gamma(\sum_{i=1}^N x_i)} \right) \left(\int_0^\infty \ln(1 + \mu_t \gamma) \gamma^{-1 + \frac{1}{t} \sum_{i=1}^N x_i} d\gamma \right) dx_i \quad (31)$$

To solve the inner integral in (31), we use [53, 01.04.07.0002.01] to express $\ln(1 + \mu_t \gamma) = \frac{1}{2\pi j} \int_{\mathcal{L}} \frac{\Gamma(u+1)\Gamma(-u)^2}{\Gamma(1-u)} (\mu_t \gamma)^{-u} du$ and use the final value theorem $\lim_{x \rightarrow \infty} \int_0^x f(u) du = \lim_{s \rightarrow 0} F(s) = F(\epsilon)$, where

$$\bar{P}_e^{\infty, \text{DL}} \approx \frac{\psi v^k}{2\Gamma(p)} \sum_{l=1}^P \zeta_l C_l^{-\phi} \left[\sum_{i=1}^m \frac{\prod_{w=1, w \neq i}^m \Gamma(b_{l,w} - b_{l,i}) (\Gamma(v - \phi - b_{l,i}))^k \prod_{w=1}^n \Gamma(1 - a_{l,w} + b_{l,i}) \Gamma(\phi + b_{l,i}) \Gamma(p + \frac{\phi + b_{l,i}}{t})}{\prod_{w=n+1}^p \Gamma(a_{l,w} - b_{l,i}) (\Gamma(v + 1 - \phi - b_{l,i}))^k \prod_{w=m+1}^q \Gamma(1 - b_{l,w} + b_{l,i}) \Gamma(1 + \phi + b_{l,i})} \right. \\ \left. \left(C_l^{\phi + b_{l,i}} \left(\frac{1}{q\gamma_0} \right)^{(\phi + b_{l,i})/t} \right) + k \frac{\prod_{w=1}^m \Gamma(\phi + b_{l,w} - v) \prod_{w=1}^n \Gamma(1 - \phi - a_{l,w} + v) \Gamma(v) \Gamma(p + \frac{v}{t})}{\prod_{w=n+1}^p \Gamma(\phi + a_{l,w} - v) \prod_{w=m+1}^q \Gamma(1 - \phi - b_{l,w} + v) \Gamma(1 + v)} \left(C_l^v \left(\frac{1}{q\gamma_0} \right)^{v/t} \right) \right] \quad (28)$$

$$\bar{\eta} = \frac{\log_2(e)}{t} \sum_{l_{1,1}, l_{1,2}=1}^P \cdots \sum_{l_{N,1}, l_{N,2}=1}^P \prod_{i=1}^N \prod_{j=1}^2 \psi_{i,j} v_{i,j}^{k_{i,j}} \zeta_{l_{i,j}} \left(C_{l_{i,j}} \right)^{-\phi_{i,j}} \\ \left[\begin{array}{c} \left(\frac{1}{\epsilon\gamma_0} \right)^{1/t} \prod_{j=1}^2 C_{l_{i,j}} \\ \vdots \\ \left(\frac{1}{\epsilon\gamma_0} \right)^{1/t} \prod_{j=1}^2 C_{l_{i,j}} \\ \frac{\mu_t}{\epsilon} \end{array} \middle| \begin{array}{l} (1, \frac{1}{t}, \dots, \frac{1}{t}, 1) : V_1; (1, 1), (1, 1) \\ (1; 1, \dots, 1, 0) : V_2; (1, 1), (0, 1) \end{array} \right] \quad (30)$$

where $V_1 = \{ \{(\phi_{i,1} + a_{l_{i,1},w}, 1)\}_{w=1}^n, \{(\phi_{i,2} + a_{l_{i,2},w}, 1)\}_{w=1}^n, (1, 1), \{(\phi_{i,1} + a_{l_{i,1},w}, 1)\}_{w=n+1}^p, \{(\phi_{i,2} + a_{l_{i,2},w}, 1)\}_{w=n+1}^p, \{(v_{i,1} + 1, 1)\}_1^{k_{i,1}}, \{(v_{i,2} + 1, 1)\}_1^{k_{i,2}} \}_{i=1}^N$ and $V_2 = \{ \{(\phi_{i,1} + b_{l_{i,1},w}, 1)\}_{w=1}^m, \{(\phi_{i,2} + b_{l_{i,2},w}, 1)\}_{w=1}^m, \{(v_{i,1}, 1)\}_1^{k_{i,1}}, \{(v_{i,2}, 1)\}_1^{k_{i,2}}, \{(\phi_{i,1} + b_{l_{i,1},w}, 1)\}_{w=m+1}^q, \{(\phi_{i,2} + b_{l_{i,2},w}, 1)\}_{w=m+1}^q \}_{i=1}^N$.

ϵ is close to zero (in the order 10^{-6}). Thus, the inner integral becomes

$$\int_0^\infty \ln(1 + \mu_t \gamma) (\gamma)^{-1 + \frac{1}{t} \sum_{i=1}^N x_i} d\gamma = \lim_{s \rightarrow 0} \frac{1}{2\pi j} \int_{\mathcal{C}} \frac{\Gamma(u+1)\Gamma(-u)^2}{\Gamma(1-u)} (\mu_t^{-u} (\frac{1}{s})^{-u + \frac{1}{t} \sum_{i=1}^N x_i} \Gamma(-u + \frac{1}{t} \sum_{i=1}^N x_i)) du \\ = \frac{1}{2\pi j} \int_{\mathcal{C}} \frac{\Gamma(u+1)\Gamma(-u)^2}{\Gamma(1-u)} (\mu_t^{-u} (\frac{1}{\epsilon})^{-u + \frac{1}{t} \sum_{i=1}^N x_i} \Gamma(-u + \frac{1}{t} \sum_{i=1}^N x_i)) d\zeta \quad (32)$$

We substitute (32) in (31) and apply the definition of N -multivariate Fox's H-function [55, A.1] to get (30). ■

We derive an exact closed form expression of the DL-FSO system by substituting (9) in (29), representing $\ln(1 + \mu_t \gamma)$ in terms of Meijer's G-function and applying the identity [53, 07.34.21.0012.01]:

$$\bar{\eta}^{\text{DL}} = \log_2(e) \frac{\psi v^k}{t} \sum_{l=1}^P \zeta_l C_l^{-\phi} \\ H_{p+k+2, q+k+2}^{m+k+2, n+1} \left[C_l \left(\frac{1}{\mu_t \gamma_0} \right)^{1/t} \middle| \begin{array}{l} V_1, (0, \frac{1}{t}), (1, \frac{1}{t}), V_2 \\ V_3, (0, \frac{1}{t}), (0, \frac{1}{t}), V_4 \end{array} \right] \quad (33)$$

where $V_1 = \{(\phi + a_{l,w}, 1)\}_{w=1}^n$, $V_2 = \{(\phi + a_{l,w}, 1)\}_{w=n+1}^p, \{(v + 1, 1)\}_1^k$, $V_3 = \{(\phi + b_{l,w}, 1)\}_{w=1}^m, \{(v, 1)\}_1^k$ and $V_4 = \{(\phi + b_{l,w}, 1)\}_{w=m+1}^q$.

D. Moments of SNR

Finally, we derive moments of SNR for both RISE-FSO and DL-FSO systems, which can be a useful metric to characterize the average SNR and order of fading.

Lemma 4. *The r -th moment of SNR for the RISE-FSO system is given as (34).*

Proof: We substitute the PDF of SNR (18) (using (14)) in $\mathbb{E}[\gamma^r] = \int_0^\infty \gamma^r f_\gamma(\gamma) d\gamma$ to compute the r -th moment of SNR by expanding the definition of Fox's H-function:

$$\bar{\gamma}^{(r)} = \frac{1}{t} \sum_{l_{1,1}, l_{1,2}=1}^P \cdots \sum_{l_{N,1}, l_{N,2}=1}^P \prod_{i=1}^N \prod_{j=1}^2 \psi_{i,j} v_{i,j}^{k_{i,j}} \zeta_{l_{i,j}} \\ (C_{l_{i,j}})^{-\phi_{i,j}} \left(\frac{1}{2\pi j} \right)^N \int_{\mathcal{C}_i} \left(\left(\frac{1}{\gamma_0} \right)^{1/t} \prod_{j=1}^2 C_{l_{i,j}} \right)^{x_i} \\ \left[\frac{\prod_{j=1}^2 \prod_{w=1}^m \Gamma(-x_i + \phi_{i,j} + b_{l_{i,j},w})}{\prod_{j=1}^2 \prod_{w=n+1}^p \Gamma(-x_i + \phi_{i,j} + a_{l_{i,j},w})} \frac{\prod_{j=1}^2 \prod_{w=1}^n \Gamma(1 + x_i - \phi_{i,j} - a_{l_{i,j},w})}{\prod_{j=1}^2 \prod_{w=m+1}^q \Gamma(1 + x_i - \phi_{i,j} - b_{l_{i,j},w})} \right. \\ \left. \frac{\prod_{j=1}^2 (\Gamma(v_{i,j} - x_i))^{k_{i,j}} \Gamma(x_i)}{\prod_{j=1}^2 (\Gamma(1 + v_{i,j} - x_i))^{k_{i,j}} \Gamma(\sum_{i=1}^N x_i)} \right] \left(\int_0^\infty \gamma^r \gamma^{-1 + \frac{1}{t} \sum_{i=1}^N x_i} d\gamma \right) dx_i \quad (35)$$

To solve inner integral in (35) we use the final value theorem:

$$\int_0^\infty (\gamma)^{r-1 + \frac{1}{t} \sum_{i=1}^N x_i} d\gamma = \left(\frac{1}{\epsilon} \right)^{r + \frac{1}{t} \sum_{i=1}^N x_i} \Gamma\left(r + \frac{1}{t} \sum_{i=1}^N x_i\right) \quad (36)$$

We substitute (36) in (35) and use the definition of N -multivariate Fox's H-function [55, A.1] to get (34). ■

Similarly, we derive an exact closed form expression of the r -th moment of SNR for the DL-FSO system by substituting (9) in $\mathbb{E}[\gamma^r] = \int_0^\infty \gamma^r f_\gamma(\gamma) d\gamma$, expand the Fox's H-function, use the final value theorem to compute the inner integral $\int_0^\infty \gamma^{r-1 + \frac{x}{t}} d\gamma = \lim_{s \rightarrow 0} (\frac{1}{s})^{r + \frac{x}{t}} \Gamma(r + \frac{x}{t}) = (\frac{1}{\epsilon})^{r + \frac{x}{t}} \Gamma(r + \frac{x}{t})$ to get (37).

In what follows, we demonstrate the performance of FSO systems using numerical and simulation analysis.

V. SIMULATION AND NUMERICAL RESULTS

In this section, we use numerical analysis and Monte Carlo simulations (averaged over 10^8 channel realizations) to demonstrate the performance of the proposed RISE-FSO

$$\bar{\gamma}^{(r)} = \mathbb{E}[\gamma^r] = \frac{1}{t} \left(\frac{1}{\epsilon} \right)^r \sum_{l_{1,1}, l_{1,2}=1}^P \cdots \sum_{l_{N,1}, l_{N,2}=1}^P \prod_{i=1}^N \prod_{j=1}^2 \psi_{i,j} v_{i,j}^{k_{i,j}} \zeta_{l_{i,j}} \left(C_{l_{i,j}} \right)^{-\phi_{i,j}}$$

$$H_{1,1:2p+k_{1,1}+k_{1,2}, 2n+1; \dots; 2m+k_{N,1}+k_{N,2}, 2n+1}^{0,1} \left[\begin{array}{c} \left(\frac{1}{\epsilon \gamma_0} \right)^{1/t} \prod_{j=1}^2 C_{l_{i,j}} \\ \vdots \\ \left(\frac{1}{\epsilon \gamma_0} \right)^{1/t} \prod_{j=1}^2 C_{l_{i,j}} \end{array} \middle| \begin{array}{l} (1-r, \frac{1}{t}, \dots, \frac{1}{t}) : V_1 \\ (1, 1, \dots, 1) : V_2 \end{array} \right] \quad (34)$$

where $V_1 = \{ \{ (\phi_{i,1} + a_{l_{i,1},w}, 1), \{ (\phi_{i,2} + a_{l_{i,2},w}, 1) \}_{w=1}^n, (1, 1), \{ (\phi_{i,1} + a_{l_{i,1},w}, 1) \}_{w=n+1}^p, \{ (\phi_{i,2} + a_{l_{i,2},w}, 1) \}_{w=n+1}^p, \{ (v_{i,1} + 1, 1) \}_1^{k_{i,1}}, \{ (v_{i,2} + 1, 1) \}_1^{k_{i,2}} \}_{i=1}^N$ and $V_2 = \{ \{ (\phi_{i,1} + b_{l_{i,1},w}, 1) \}_{w=1}^m, \{ (\phi_{i,2} + b_{l_{i,2},w}, 1) \}_{w=1}^m, \{ (v_{i,1}, 1) \}_1^{k_{i,1}}, \{ (v_{i,2}, 1) \}_1^{k_{i,2}}, \{ (\phi_{i,1} + b_{l_{i,1},w}, 1) \}_{w=m+1}^q, \{ (\phi_{i,2} + b_{l_{i,2},w}, 1) \}_{w=m+1}^q \}_{i=1}^N$.

$$\bar{\gamma}^{(r, \text{DL})} = \mathbb{E}[\gamma^r] = \frac{\psi v^k}{t} \left(\frac{1}{\epsilon} \right)^r \sum_{l=1}^P \zeta_l C_l^{-\phi} H_{p+k+1, q+k}^{m+k, n+1}$$

$$\left[C_l \left(\frac{1}{\epsilon \gamma_0} \right)^{1/t} \middle| \begin{array}{l} (1-r, \frac{1}{t}), \{ (\phi + a_{l,w}, 1) \}_{w=1}^n, \{ (\phi + a_{l,w}, 1) \}_{w=n+1}^p, \{ (v+1, 1) \}_1^k \\ \{ (\phi + b_{l,w}, 1) \}_{w=1}^m, \{ (v, 1) \}_1^k, \{ (\phi + b_{l,w}, 1) \}_{w=m+1}^q \end{array} \right] \quad (37)$$

TABLE IV
SIMULATION PARAMETERS

Transmitted power, P_T	0 to 40 dBm	Responsivity, R	0.41 A/W
AWGN variance, σ_ν^2	10^{-14} A ² /GHz	Link distance, $\{d\}$	{1 km, 2 km}
Visibility range, V	2 km	Aperture diameter, $D = 2a_r$	20 cm
Shape parameter of fog, k	{2, 5}	Scale parameter of fog, β^{fog}	{13.12, 12.06}
Normalized beam-width, w_z/a_r	{10, 15}	Normalized jitter, σ_s/a_r	3
Pointing error angle σ_θ standard deviation,	1 mrad	RIS jitter angle σ_β standard deviation,	0.5 mrad
Modulation, DBPSK	$p = 1, q = 1$	Wavelength, λ	1550 nm
Refractive index, C_n^2	$\{5 \times 10^{-14}, 1.25 \times 10^{-14}\} m^{-2/3}$	\mathcal{F} -distribution, $\{\alpha_F, \beta_F\}$	{4.85, 6.55}, {17.21, 19.24} {17.48, 17.8}, {68.14, 64.73}
\mathcal{GG} -distribution, $\{\alpha_G, \beta_G\}$	{3.01, 3}, {8.9, 12}, {8.17, 11}, {30.76, 40}	\mathcal{M} -distribution, $\{\alpha_M, \beta_M, \Omega, b_0, \rho\}$	{3.01, 3, 0.4, 0.3, 0.596}, {8.9, 12, 0.4, 0.3, 0.596}, {8.17, 11, 0.4, 0.3, 0.596}, {30.76, 40, 0.4, 0.3, 0.596}

system under the combined effect of atmospheric turbulence and pointing errors over different weather conditions. We also compare the performance of DL-FSO and RISE-FSO systems using both HD and IM/DD detection techniques. We evaluate the derived analytical expressions using the Python code implementation of multivariate Fox's H-function [56] and validate them through extensive numerical and simulation results. The computational complexity of Fox's H-function depends more on the number of contour integrals than the computation of integrand involving Gamma functions. Thus, numerical evaluation of the single-variate Fox's H-function is fast since it requires the computation of a single contour involving the ratio of products of $m+n$ and $p+q$ Gamma functions even for large values of m, n, p , and q . However, the computation of an N -variate Fox's H-function becomes slower with an increase in the number of contour integrals, N . We assume link distances of $d = 1\text{km}$ and $d = 2\text{km}$ for weather conditions of fog and haze, respectively. We assume that the optical RIS is situated midway between the source

and the destination i.e., $d_1 = d_2 = d/2$. We use parametric equations to compute \mathcal{F} -turbulence parameters from [47], \mathcal{GG} parameters from [57], and use $\alpha_M = \alpha_G$ and $\beta_M = \beta_G$ for the \mathcal{M} distribution with Ω, b_0 , and ρ [10]. We use the recent paper [28] to model pointing errors for optical RIS. We list simulation parameters in Table IV.

In what follows, we demonstrate the performance of DL-FSO and RISE-FSO systems in next two subsections.

A. DL-FSO system

We demonstrate the performance of DL-FSO system in Fig. 2 and Fig. 3 by plotting average SNR, ergodic capacity, outage probability, and average BER with HD and IM/DD detection under the combined effect of atmospheric turbulence, pointing errors, and foggy conditions. Observing these figures, it can be seen that the HD detector outperforms IM/DD for the considered atmospheric turbulence models at the expense of decoding complexity. Fig. 2(a) shows that the average SNR is reduced by almost 35dB and 25dB at a transmit power of

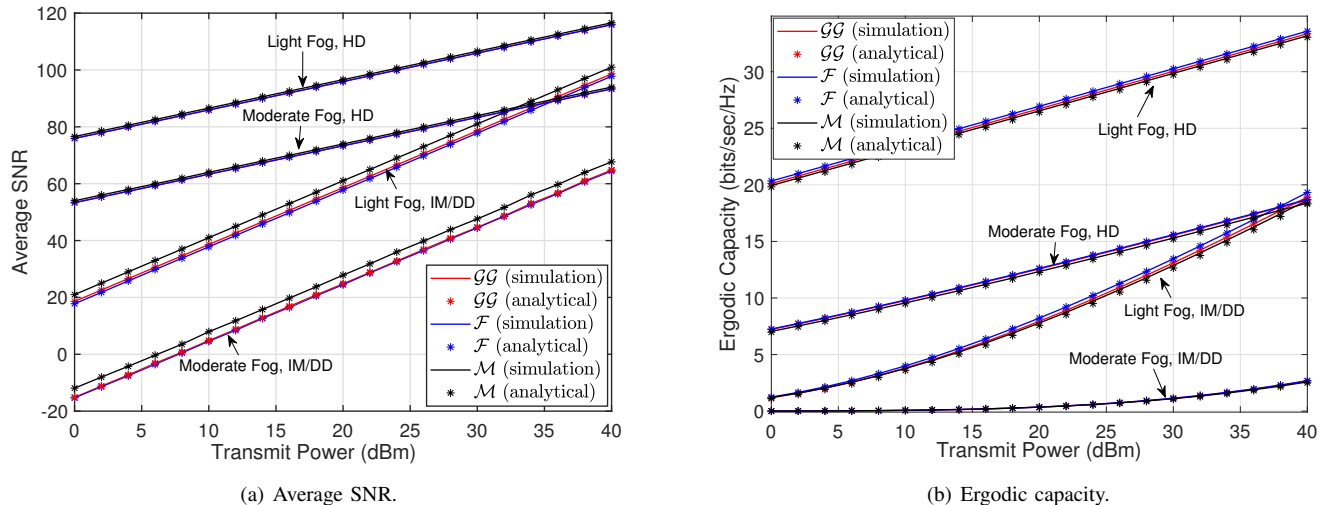


Fig. 2. Average SNR and ergodic capacity of DL-FSO at $d = 1\text{km}$ for light and moderate fog with HD and IM/DD detection.

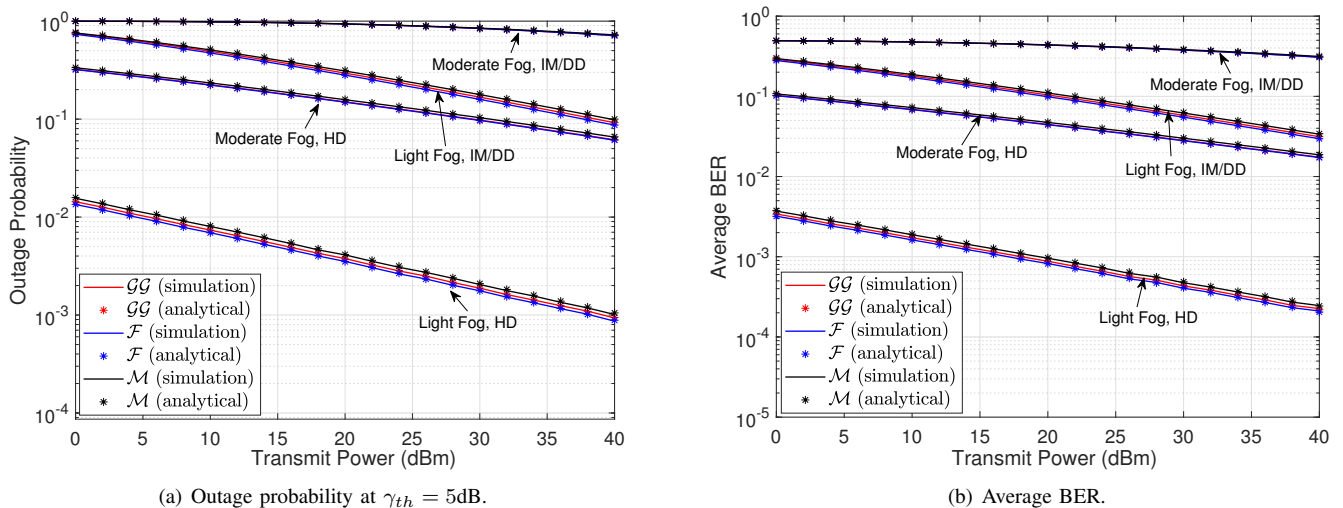


Fig. 3. Outage probability and average BER for DL-FSO system at $d = 1\text{km}$ with HD and IM/DD detection for light and moderate fog.

20dBm over moderate foggy conditions compared with light foggy for IM/DD and HD detection techniques, respectively. Further, it can be seen from Fig. 2(b) that the moderate fog has a more cumulative impact on IM/DD than the HD detection. The figure depicts that the ergodic capacity has a factor of 6 reductions for the IM/DD but with a factor 2 reduction comparing light foggy weather to the moderate fog at a transmit power of 40dBm. It can also be seen that the performance of FSO system is significantly degraded for back-haul applications over moderate foggy conditions, especially with the IM/DD technique. The outage probability and average BER performance of the DL-FSO system are illustrated in Fig. 3. Despite the fact that the HD detector performs better than the IM/DD, the outage probability and average BER performance is significantly degraded to around 10^{-1} at a higher transmit $P_T = 40\text{dBm}$ for moderate foggy conditions at a link distance of 1km. Acceptable reliability of 10^{-3} can only be achieved for light foggy conditions with

HD detection. A further decrease in link distance, say 500m, may improve the reliability of transmissions for a good quality of service. Considering parameters of atmospheric turbulence (using Table IV) and pointing errors ($\rho^2 = 2.25$), we can use our analysis to derive the diversity order for the considered DL-FSO system as $\frac{0.33}{t}$ and $\frac{0.36}{t}$ for light and moderate fog, respectively. Fig. 3 confirms the derived diversity order since there is no change in the slope for different turbulence models, almost same slope for similar detection methods for both foggy conditions, and a change in the slope comparing the plots for HD ($t = 1$) and IM/DD ($t = 2$). Thus, the diversity order provides design criteria to appropriately choose the beamwidth to reduce the impact of pointing errors on FSO systems with other channel impairments. It can also be seen from Fig. 3(b) that analytical expressions and simulation results for the considered binary modulation scheme have an excellent match over a wide range of SNR. In the following subsection, we employ the optical RIS to improve the performance of the

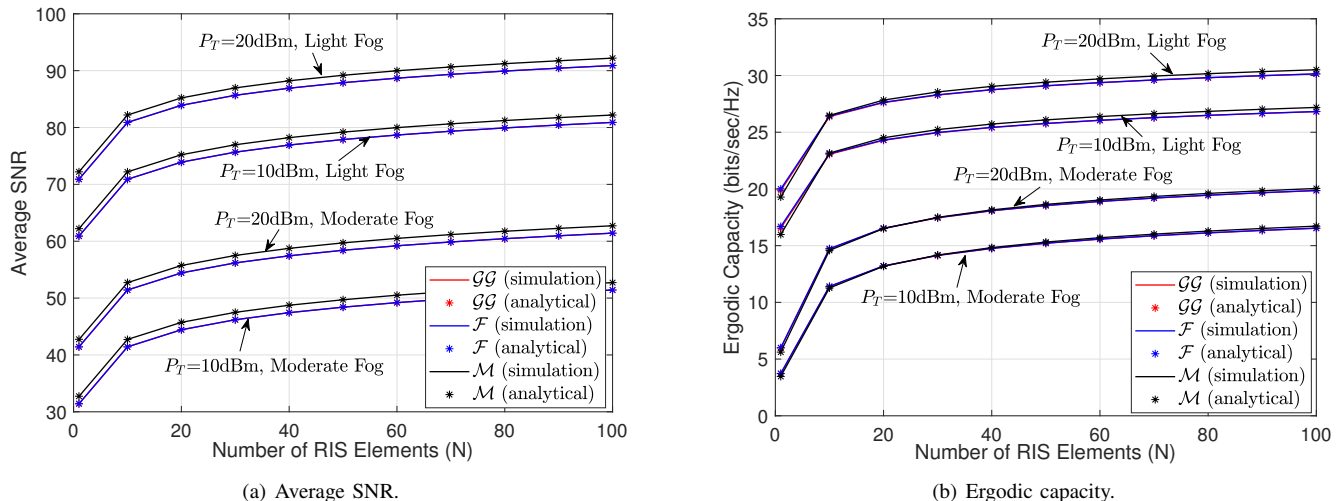


Fig. 4. Average SNR and ergodic capacity of RISE-FSO system at $d_1 = 500\text{m}$, and $d_2 = 500\text{m}$ with HD for light and moderate fog.

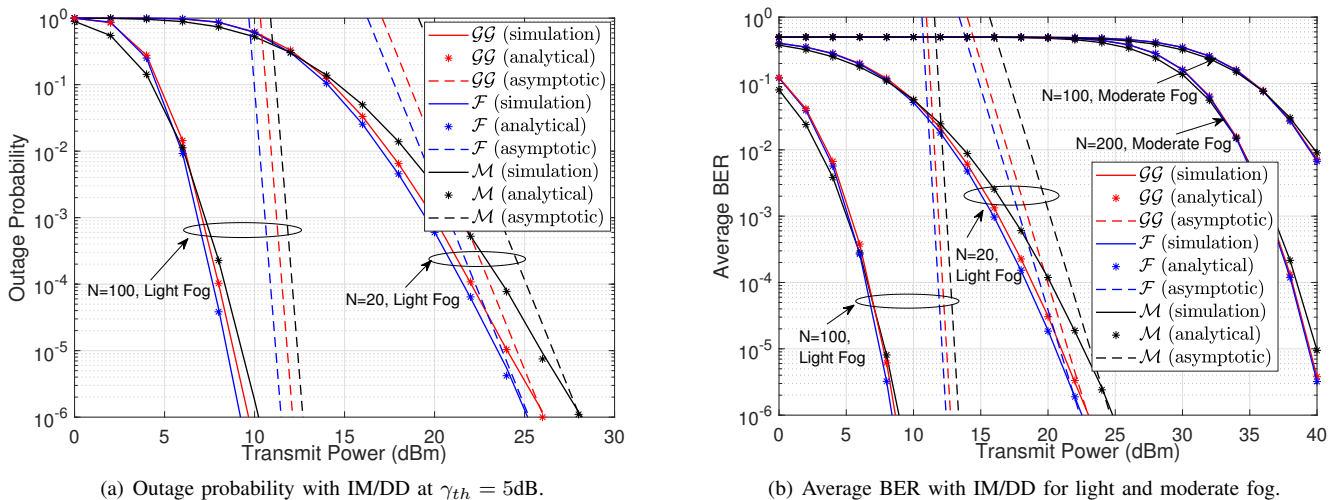


Fig. 5. Outage probability and average BER of RISE-FSO system at $d_1 = 500\text{m}$, and $d_2 = 500\text{m}$.

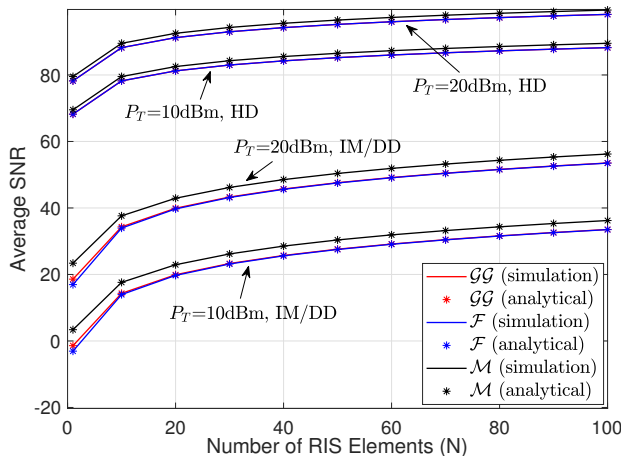
DL-FSO system.

B. RISE-FSO system

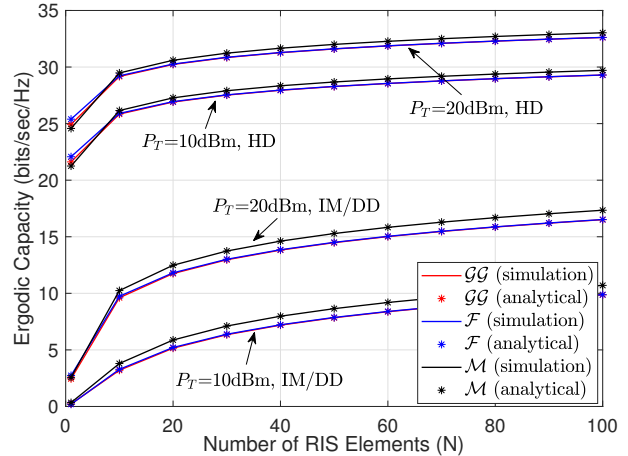
We use parameters for atmospheric turbulence and pointing errors customized for the optical RIS to simulate the RISE-FSO system, as listed in Table IV. Without loss of generality, we assume i.i.d channel model for both the hops by considering the same parameters of the atmospheric turbulence, random fog, and pointing errors from source to the RIS and RIS to the destination. In Fig. 4, we demonstrate the impact of RIS elements on the average SNR and ergodic capacity for light and moderate fog with HD technique at a transmit power of 10dBm and 20dBm. It can be seen that average SNR and ergodic capacity increase with an increase in the number of RIS elements. Compared with the RISE-FSO, the average SNR for the DL-FSO system is higher than the $N = 100$ RIS system. However, comparing the ergodic capacity of RISE-FSO in Fig. 4(b) with the DL-FSO in Fig. 2(b), we can observe

that a 100 element RIS surface can provide a significant increase of 3 bits/sec/Hz in spectral efficiency.

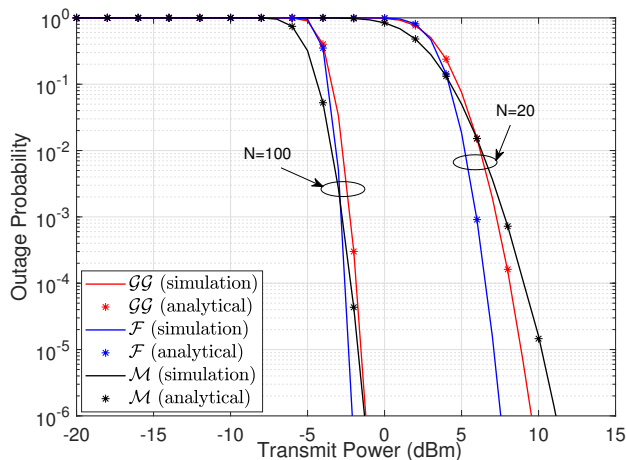
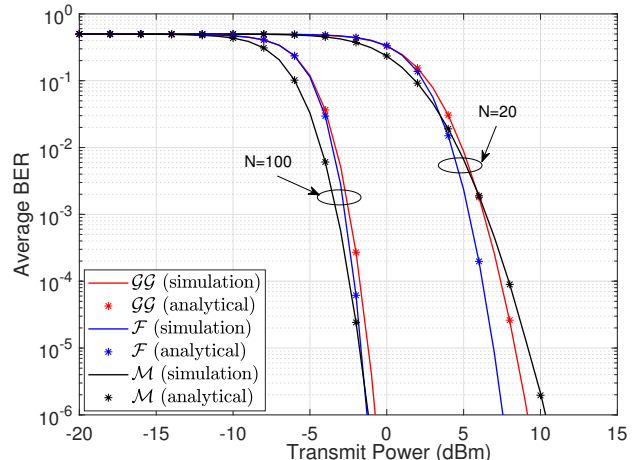
There is a significantly higher improvement in the performance of outage probability and average BER with RIS, as shown in Fig. 5. We demonstrate the impact of RIS elements on these performance metrics for light and moderate fog conditions with the IM/DD detector. Fig. 5(a) shows that the $N = 100$ RISE-FSO achieves a gain of about 12dBm of transmit power to achieve the same outage probability of 10^{-3} compared with the $N = 20$ RIS system under light fog conditions. Further, we can verify the impact of RIS elements on the diversity order of RISE-FSO system as predicted through analytical results. In Fig. 5(b), we plot the average BER of the RISE-FSO system for both light and moderate foggy conditions. The figure shows that the average BER improves significantly with an increase in the number of RIS elements. Moreover, the behavior of slope in the average BER with N depicts the diversity gain of the RISE-FSO



(a) Average SNR with HD and IM/DD.



(b) Ergodic capacity with HD and IM/DD.

Fig. 6. Average SNR and ergodic capacity of RISE-FSO system with deterministic path loss at $d_1 = 1\text{km}$, $d_2 = 1\text{km}$, and $C_n^2 = 5 \times 10^{-14} \text{m}^{-2/3}$.(a) Outage probability with IM/DD at $\gamma_{th} = 5\text{dB}$.

(b) Average BER with IM/DD.

Fig. 7. Outage probability and average BER of RISE-FSO system with deterministic path loss at $d_1 = 1\text{km}$, $d_2 = 1\text{km}$, and $C_n^2 = 5 \times 10^{-14} \text{m}^{-2/3}$.

system. We also verify the slope of the BER and the outage probability at high SNR by plotting the numerically evaluated derived asymptotic expressions for both outage probability and average BER for light foggy conditions. It can also be seen from Fig. 5(b) that the average BER for the moderate fog condition is still higher even with $N = 100$ RIS elements, the performance degradation caused by moderate fog can be compensated with a further increase in N (as seen with the plot $N = 200$ in Fig. 5(b)). Thus, it is possible to reduce the effect of atmospheric turbulence, pointing errors, and adverse weather conditions by increasing the number of RIS elements demonstrating a potential design criteria for terrestrial FSO systems.

Finally, we consider the conventional FSO communications over atmospheric turbulence and pointing errors with deterministic path loss evaluated using the well known Beer-Lambert's law and visibility range. In Fig. 6 and Fig. 7, we use

similar simulation parameters of the RISE-FSO with random fog to perform experiments on the average SNR, ergodic capacity, and outage probability, average BER of the RISE-FSO by considering non-foggy condition with a visibility range of haze conditions. Fig. 6 and Fig. 7 demonstrate that there is an improvement in the FSO system due to lower path loss with a higher visibility range of haze conditions. Further, figures show that the impact of RIS elements on the performance of RISE-FSO without fog follows a similar trend to that of the RISE-FSO with fog, as described in the preceding paragraphs.

In all the above figures (Fig. 2 to Fig. 7), it can be seen that our derived unified expressions have a good agreement with Monte-Carlo simulations validating the proposed analysis. Moreover, the performance of the FSO system is similar for \mathcal{F} , \mathcal{GG} , and \mathcal{M} models since the turbulence scenarios (i.e., from medium to strong as depicted by the respective turbulence

parameters) are applicable for the three atmospheric models. However, \mathcal{F} , \mathcal{GG} slightly overestimates the performance for very strong turbulence compared with \mathcal{M} -distribution.

VI. CONCLUSIONS

In this paper, we presented exact closed-form expressions on the performance of RIS empowered FSO system under various channel impairments such as atmospheric turbulence, pointing errors, and different weather conditions. Our derived analytical results are unified, allowing evaluation of the RISE-FSO system over \mathcal{F} , \mathcal{GG} , and \mathcal{M} atmospheric turbulence models with pointing errors, deterministic and random path-loss, and considering both HD and IM/DD detection techniques. We developed an exact analysis of the performance metrics such as outage probability, average BER, ergodic capacity, and moments of SNR of the RISE-FSO system. Using the asymptotic analysis on the outage probability and average BER, we derived the diversity order, which provides different design criteria to circumvent the effect of pointing errors and random fog for the FSO system under atmospheric turbulence using the proposed RIS based solution. As such, an increase in the RIS elements significantly improve the FSO performance with non-LOS transmission link, whereas the use of suitable beamwidth mitigates the impact of pointing errors, and limiting the communication range is useful for reducing the effect of random fog. We provided extensive simulations and numerical analysis to demonstrate the effectiveness of the RISE-FSO system comparing with the DL-FSO under various channel conditions. Simulation plots provide various design configurations of system and channel parameters to achieve the desired performance. It has been shown that the performance degradation caused by atmospheric turbulence, pointing errors, and adverse weather conditions can be compensated by increasing the number of RIS elements. The proposed work demonstrated the application of optical RIS to enhance the performance of the FSO system considering a general scenario of atmospheric turbulence, pointing error impairments, weather conditions, and the underlying detection methods. We envision that the RIS technology can empower the deployment of the FSO system for next generation wireless networks, especially for terrestrial applications.

As a future scope, it would be interesting to combine the RISE-FSO system with RIS-assisted RF for better connectivity in the access network. Further, we may extend the single-RIS based system to multi-RIS for enhanced performance. Analysis of the system performance with imperfect phase compensation at the RIS may also be conducted.

APPENDIX A: PDF AND CDF OF DIRECT LINK h_i

We use the joint distribution of conditional random variables to get the PDF of $h_i = h_i^{(tp)} h_i^{(f)}$ as [50]:

$$f_{h_i}(x) = \int_x^\infty \frac{f_{h_i^{(f)}}\left(\frac{x}{u}\right) f_{h_i^{(tp)}}(u)}{u} du \quad (38)$$

where the limits of the integral are selected using the inequalities $0 \leq \frac{x}{u} \leq 1$ and $0 \leq u \leq \infty$ since $h_i^{(f)} \in [0, 1]$ and $h_i^{(t)} \in [0, \infty)$. Using (6) and (8) in (38), we get

$$f_{h_i}(x) = \psi \frac{v^k}{\Gamma(k)} \sum_{l=1}^P \zeta_l x^{v-1} \int_x^\infty u^{\phi-1} \frac{\ln^{k-1}\left(\frac{u}{x}\right)}{u^v} G_{p,q}^{m,n} \left[C_l u \left| \begin{matrix} \{a_{l,w}\}_{w=1}^p \\ \{b_{l,w}\}_{w=1}^q \end{matrix} \right. \right] du \quad (39)$$

We use the definition of Meijer's G-function, interchange the order of integration to express (39) as

$$f_{h_i}(x) = \psi \frac{v^k}{\Gamma(k)} \sum_{l=1}^P \zeta_l x^{v-1} \frac{1}{2\pi j} \int_{\mathcal{L}} \left(C_l \right)^s \frac{\prod_{j=1}^m \Gamma(b_{l,j} - s)}{\prod_{j=n+1}^p \Gamma(a_{l,j} - s)} \frac{\prod_{j=1}^n \Gamma(1 - a_{l,j} + s)}{\prod_{j=m+1}^q \Gamma(1 - b_{l,j} + s)} \left(\int_x^\infty u^{\phi-v-1} \ln^{k-1} \left(\frac{u}{x} \right) u^s du \right) ds \quad (40)$$

Substituting $\ln\left(\frac{u}{x}\right) = y$ and applying $\frac{1}{v-s-\phi} = \frac{\Gamma(v-s-\phi)}{\Gamma(v-s-\phi+1)}$, the inner integral in (40) can be solved as

$$\begin{aligned} & \int_x^\infty u^{s+\phi-v-1} \ln^{k-1} \left(\frac{u}{x} \right) du \\ &= \frac{x^{s+\phi-v} (\Gamma(v-s-\phi+1))^k}{(\Gamma(v-s-\phi))^k} \Gamma(k) \end{aligned} \quad (41)$$

Finally, we use (41) in (40) and apply the definition of Meijer's G-function, we get (9) of Theorem 1. To derive the CDF, we use the following:

$$\begin{aligned} F_{h_i}(x) &= \int_0^x f_{h_i}(u) du = \psi v^k \sum_{l=1}^P \zeta_l \\ & \frac{1}{2\pi j} \int_{\mathcal{L}} \frac{\prod_{j=1}^m \Gamma(b_{l,j} - s) \prod_{j=1}^n \Gamma(1 - a_{l,j} + s)}{\prod_{j=n+1}^p \Gamma(a_{l,j} - s) \prod_{j=m+1}^q \Gamma(1 - b_{l,j} + s)} \\ & \frac{(\Gamma(v-s-\phi))^k}{(\Gamma(v-s-\phi+1))^k} (C_l)^s \left(\int_0^x v^{s+\phi-1} dv \right) ds \end{aligned} \quad (42)$$

Using the solution of inner integral $\int_0^x v^{s+\phi-1} dv = \frac{x^{s+\phi}}{s+\phi} = x^{s+\phi} \frac{\Gamma(s+\phi)}{\Gamma(s+\phi+1)}$ in (42), we apply the definition of Meijer's G-function to get (10).

As a sanity check, we verify the derived PDF by considering the \mathcal{F} -turbulence scenario. Thus, we use parameters from Table II for the \mathcal{F} -distribution and apply the identity [53, 07.34.21.0009.01]:

$$\begin{aligned} \int_0^\infty f_{h_i}(x) dx &= \frac{\alpha_F \rho^2 v^k}{(\beta_F - 1) A_0 \Gamma(\alpha_F) \Gamma(\beta_F)} \\ \int_0^\infty G_{k+2, k+2}^{k+2, 1} \left[\frac{\alpha_F}{(\beta_F - 1) A_0} x \left| \begin{matrix} -\beta_F, \rho^2, \{v\}_1^k \\ \alpha_F - 1, \rho^2 - 1, \{v-1\}_1^k \end{matrix} \right. \right] dx \\ &= \frac{\alpha_F \rho^2 v^k}{(\beta_F - 1) A_0 \Gamma(\alpha_F) \Gamma(\beta_F)} \frac{\Gamma(\alpha_F) \Gamma(\rho^2) (\Gamma(v))^k \Gamma(\beta_F)}{\Gamma(1 + \rho^2) (\Gamma(1 + v))^k} \frac{(\beta_F - 1) A_0}{\alpha_F} \\ &= 1 \end{aligned} \quad (43)$$

APPENDIX B: PDF, CDF, AND MGF OF Z_i

We use the Mellin transform to derive the PDF of $Z_i = \prod_{j=1}^L h_{i,j}$. Here, $h_{i,j}$, $j = 1, 2, \dots, L$ are considered to be i.i.n.d random variables distributed according to (9). Thus, the PDF of Z_i :

$$f_{Z_i}(x) = \frac{1}{x} \frac{1}{2\pi j} \int_{\mathcal{L}} \mathbb{E}[Z_i^r] x^{-r} dr \quad (44)$$

where $\mathbb{E}[Z_i^r] = \prod_{j=1}^L \mathbb{E}[h_{i,j}^r] = \prod_{j=1}^L \int_0^\infty u^r f_{h_{i,j}}(u) du$ is the r -th moment of Z_i . Here, \mathcal{L} is an infinite contour in the complex r -plane such that the integrand in (44) has no singularities [55]. We substitute the PDF of $h_{i,j}$ and use the identity [53, 07.34.21.0009.01] to get

$$\begin{aligned} \int_0^\infty u^r f_{h_{i,j}}(u) du &= \psi_j v_j^{k_j} \sum_{l_j=1}^P \zeta_{l_j} \int_0^\infty u^r u^{\phi_j-1} \\ &G_{p+k_j, q+k_j}^{m+k_j, n} \left[C_{l_j} u \left| \begin{array}{c} \{a_{l_j, w}\}_{w=1}^p, \{v - \phi_j + 1\}_1^{k_j} \\ \{b_{l_j, w}\}_{w=1}^q, \{v - \phi_j\}_1^{k_j}, \{b_{l_j, w}\}_{w=m+1}^q \end{array} \right. \right] du \\ &= \psi_j v_j^{k_j} \sum_{l_j=1}^P \zeta_{l_j} (C_{l_j})^{-(r+\phi_j)} \left[\frac{\prod_{w=1}^m \Gamma(r + \phi_j + b_{l_j, w})}{\prod_{w=r+1}^p \Gamma(r + \phi_j + a_{l_j, w})} \right. \\ &\left. \frac{\prod_{w=1}^n \Gamma(1 - r - \phi_j - a_{l_j, w}) \Gamma(v_j + r)^{k_j}}{\prod_{w=m+1}^q \Gamma(1 - r - \phi_j - b_{l_j, w}) \Gamma(1 + v_j + r)^{k_j}} \right] \end{aligned} \quad (45)$$

Thus, the r -th moment of Z_i is given by

$$\begin{aligned} \mathbb{E}[Z_i^r] &= \sum_{l_1, \dots, l_L=1}^P \prod_{j=1}^L \psi_j v_j^{k_j} \zeta_{l_j} \prod_{j=1}^L (C_{l_j})^{-(r+\phi_j)} \\ &\left[\frac{\prod_{j=1}^L \prod_{w=1}^m \Gamma(r + \phi_j + b_{l_j, w})}{\prod_{j=1}^L \prod_{w=n+1}^p \Gamma(r + \phi_j + a_{l_j, w})} \right. \\ &\left. \frac{\prod_{j=1}^L \prod_{w=1}^n \Gamma(1 - r - \phi_j - a_{l_j, w}) \prod_{j=1}^L \Gamma(v_j + r)^{k_j}}{\prod_{j=1}^L \prod_{w=m+1}^q \Gamma(1 - r - \phi_j - b_{l_j, w}) \prod_{j=1}^L \Gamma(1 + v_j + r)^{k_j}} \right] \end{aligned} \quad (46)$$

We substitute (46) in (44) to get the PDF of Z_i as

$$\begin{aligned} f_{Z_i}(x) &= \frac{1}{x} \frac{1}{2\pi j} \sum_{l_1, \dots, l_L=1}^P \prod_{j=1}^L \psi_j v_j^{k_j} \zeta_{l_j} (C_{l_j})^{-\phi_j} \int_{\mathcal{L}} \left(x \prod_{j=1}^L C_{l_j} \right)^{-r} \\ &\left[\frac{\prod_{j=1}^L \prod_{w=1}^m \Gamma(r + \phi_j + b_{l_j, w})}{\prod_{j=1}^L \prod_{w=n+1}^p \Gamma(r + \phi_j + a_{l_j, w})} \right. \\ &\left. \frac{\prod_{j=1}^L \prod_{w=1}^n \Gamma(1 - r - \phi_j - a_{l_j, w}) \prod_{j=1}^L \Gamma(v_j + r)^{k_j}}{\prod_{j=1}^L \prod_{w=m+1}^q \Gamma(1 - r - \phi_j - b_{l_j, w}) \prod_{j=1}^L \Gamma(1 + v_j + r)^{k_j}} \right] dr \end{aligned} \quad (47)$$

The region of convergence of the contour integral \mathcal{L} depends on $\arg(x \prod_{j=1}^L C_{l_j})$ and $\delta = m + n - \frac{p+q}{2}$, which is the entire plane if $\arg(x \prod_{j=1}^L C_{l_j}) \leq \delta\pi$ [53, 07.34.02.0001.01]. Since $\delta = 1$ and $\arg(x \prod_{j=1}^L C_{l_j}) = 0$, the region of the contour integral in (47) is $\mathcal{L} : -j\infty \rightarrow +j\infty$.

Hence, we apply the definition of Meijer's G-function in (47) to get (11). The CDF of Z_i can be obtained as $F_{Z_i}(x) = \int_0^x f_{Z_i}(u) du$. Thus,

$$\begin{aligned} F_{Z_i}(x) &= \frac{1}{2\pi j} \sum_{l_1, \dots, l_L=1}^P \prod_{j=1}^L \psi_j v_j^{k_j} \zeta_{l_j} (C_{l_j})^{-\phi_j} \int_{\mathcal{L}} \left(\prod_{j=1}^L C_{l_j} \right)^r \\ &\left(\int_0^x u^{r-1} du \right) \left[\frac{\prod_{j=1}^L \prod_{w=1}^m \Gamma(-r + \phi_j + b_{l_j, w})}{\prod_{j=1}^L \prod_{w=n+1}^p \Gamma(-r + \phi_j + a_{l_j, w})} \right. \\ &\left. \frac{\prod_{j=1}^L \prod_{w=1}^n \Gamma(1 + r - \phi_j - a_{l_j, w}) \prod_{j=1}^L \Gamma(v_j - r)^{k_j}}{\prod_{j=1}^L \prod_{w=m+1}^q \Gamma(1 + r - \phi_j - b_{l_j, w}) \prod_{j=1}^L \Gamma(1 + v_j - r)^{k_j}} \right] dr \end{aligned} \quad (48)$$

Using the inner integral solved by the identity [58, 8.331.3] $\int_0^x u^{r-1} du = \left(\frac{1}{r}\right)x^r = \frac{\Gamma(r)}{\Gamma(r+1)}x^r$ in (48) and apply the definition of Meijer's G-function to get (12).

Similarly, the MGF of Z_i $M_{Z_i}(s) = \mathbb{E}[e^{-sx}] = \int_0^\infty e^{-sx} f_{Z_i}(x) dx$ can be expressed as

$$\begin{aligned} M_{Z_i}(s) &= \frac{1}{2\pi j} \sum_{l_1, \dots, l_L=1}^P \prod_{j=1}^L \psi_j v_j^{k_j} \zeta_{l_j} (C_{l_j})^{-\phi_j} \int_{\mathcal{L}} \left(\prod_{j=1}^L C_{l_j} \right)^r \\ &\left(\int_0^\infty e^{-sx} x^{r-1} dx \right) \left[\frac{\prod_{j=1}^L \prod_{w=1}^m \Gamma(-r + \phi_j + b_{l_j, w})}{\prod_{j=1}^L \prod_{w=n+1}^p \Gamma(-r + \phi_j + a_{l_j, w})} \right. \\ &\left. \frac{\prod_{j=1}^L \prod_{w=1}^n \Gamma(1 + r - \phi_j - a_{l_j, w}) \prod_{j=1}^L \Gamma(v_j - r)^{k_j}}{\prod_{j=1}^L \prod_{w=m+1}^q \Gamma(1 + r - \phi_j - b_{l_j, w}) \prod_{j=1}^L \Gamma(1 + v_j - r)^{k_j}} \right] dr \end{aligned} \quad (49)$$

Substituting the inner integral solution using [58, 3.381.4] as $\int_0^\infty e^{-sx} x^{r-1} dx = s^{-r} \Gamma(r)$ in (49), we apply the definition of Meijer's G-function to get (13).

APPENDIX C: PDF AND CDF OF Z

We apply the inverse Laplace transform of the MGF to find the PDF of $Z = \sum_{i=1}^N Z_i$ as $f_Z(z) = \mathcal{L}^{-1} \prod_{i=1}^N M_{Z_i}(s)$. Thus, we use (49) and interchange the order of integration to get

$$\begin{aligned} f_Z(x) &= \sum_{l_{1,1}, \dots, l_{1,L}=1}^P \cdots \sum_{l_{N,1}, \dots, l_{N,L}=1}^P \prod_{i=1}^N \prod_{j=1}^L \psi_{i,j} v_{i,j}^{k_{i,j}} \zeta_{l_{i,j}} (C_{l_{i,j}})^{-\phi_{i,j}} \\ &\left(\left(\frac{1}{2\pi j} \right)^N \int_{\mathcal{L}_i} \left(\prod_{j=1}^L C_{l_{i,j}} \right)^{n_i} \left[\frac{\prod_{j=1}^L \prod_{w=1}^m \Gamma(-n_i + \phi_{i,j} + b_{l_{i,j}, w})}{\prod_{j=1}^L \prod_{w=n+1}^p \Gamma(-n_i + \phi_{i,j} + a_{l_{i,j}, w})} \right. \right. \\ &\left. \frac{\prod_{j=1}^L \prod_{w=1}^n \Gamma(1 + n_i - \phi_{i,j} - a_{l_{i,j}, w}) \prod_{j=1}^L \Gamma(v_{i,j} - n_i)^{k_{i,j}}}{\prod_{j=1}^L \prod_{w=m+1}^q \Gamma(1 + n_i - \phi_{i,j} - b_{l_{i,j}, w}) \prod_{j=1}^L \Gamma(1 + v_{i,j} - n_i)^{k_{i,j}}} \right. \\ &\left. \Gamma(n_i) \right] \left(\frac{1}{2\pi j} \int_{\mathcal{L}} s^{-\sum_{i=1}^N n_i} e^{sx} ds \right) dn_i \end{aligned} \quad (50)$$

where \mathcal{L}_i is an infinite contour in the complex n_i -plane such that the integrand in (50) has no singularities. The convergence conditions of multiple contour integrals representing multivariate Fox's H-function is presented in [59]. To solve the inner integral, we apply [58, 8.315.1]:

$$\int_{\mathcal{L}} s^{\sum_{i=1}^N n_i} e^{sx} ds = \left(\frac{1}{x} \right)^{1 + \sum_{i=1}^N n_i} \frac{2\pi j}{\Gamma(-\sum_{i=1}^N n_i)} \quad (51)$$

Using (51) in (50) and applying the definition of N -Multivariate Fox's H-function in [55, A.1], we get (14).

To derive the CDF, we use $F_Z(z) = \mathcal{L}^{-1} \prod_{i=1}^N \frac{M_{Z_i}(s)}{s}$ in (49) to get

$$\begin{aligned} F_Z(x) &= \sum_{l_{1,1}, \dots, l_{1,L}=1}^P \cdots \sum_{l_{N,1}, \dots, l_{N,L}=1}^P \prod_{i=1}^N \prod_{j=1}^L \psi_{i,j} v_{i,j}^{k_{i,j}} \zeta_{l_{i,j}} (C_{l_{i,j}})^{-\phi_{i,j}} \\ &\left(\left(\frac{1}{2\pi j} \right)^N \int_{\mathcal{L}_i} \left(\prod_{j=1}^L C_{l_{i,j}} \right)^{n_i} \left[\frac{\prod_{j=1}^L \prod_{w=1}^m \Gamma(-n_i + \phi_{i,j} + b_{l_{i,j}, w})}{\prod_{j=1}^L \prod_{w=n+1}^p \Gamma(-n_i + \phi_{i,j} + a_{l_{i,j}, w})} \right. \right. \\ &\left. \frac{\prod_{j=1}^L \prod_{w=1}^n \Gamma(1 + n_i - \phi_{i,j} - a_{l_{i,j}, w}) \prod_{j=1}^L \Gamma(v_{i,j} - n_i)^{k_{i,j}}}{\prod_{j=1}^L \prod_{w=m+1}^q \Gamma(1 + n_i - \phi_{i,j} - b_{l_{i,j}, w}) \prod_{j=1}^L \Gamma(1 + v_{i,j} - n_i)^{k_{i,j}}} \right. \\ &\left. \Gamma(n_i) \right] \left(\frac{1}{2\pi j} \int_{\mathcal{L}} s^{-1 - \sum_{i=1}^N n_i} e^{sx} ds \right) dn_i \end{aligned} \quad (52)$$

$$\int_0^\infty f_Z(z)dz = \lim_{s \rightarrow 0} \prod_{i=1}^N \prod_{j=1}^L \frac{\rho_{i,j}^2 v_{i,j}^{k_{i,j}}}{\Gamma(\alpha_F(i,j))\Gamma(\beta_F(i,j))} H_{0,0:2L+\sum_{j=1}^L k_{1,j}; \dots; L+1,2L+\sum_{j=1}^L k_{N,j}}^{0,0:2L+\sum_{j=1}^L k_{1,j}, 2L+\sum_{j=1}^L k_{1,j}+1; \dots; 2L+\sum_{j=1}^L k_{N,j}, 2L+\sum_{j=1}^L k_{N,j}+1} \left[\begin{array}{c} s \prod_{j=1}^L \frac{(\beta_F(i,j)-1)h_l A_0}{\alpha_F(i,j)} \\ \vdots \\ s \prod_{j=1}^L \frac{(\beta_F(i,j)-1)h_l A_0}{\alpha_F(i,j)} \end{array} \middle| \begin{array}{l} - : \{ \{ (1 - \alpha_F(i,j), 1) \}_{j=1}^L, \{ (1 - \rho_{i,j}^2, 1) \}_{j=1}^L, \{ \{ (1 - v_{i,j}, 1) \}_1^{k_{i,j}} \}_{j=1}^L \}_{i=1}^N \\ - : \{ (0, 1), \{ (\beta_F(i,j), 1) \}_{j=1}^L, \{ (-\rho_{i,j}^2, 1) \}_{j=1}^L, \{ \{ (-v_{i,j}, 1) \}_1^{k_{i,j}} \}_{j=1}^L \}_{i=1}^N \end{array} \right] \quad (53)$$

We apply [58, 8.315.1] to solve the inner integral in (52):

$$\int_{\mathcal{L}} s^{-1-\sum_{i=1}^N n_i} e^{sx} ds = \left(\frac{1}{x}\right)^{-\sum_{i=1}^N n_i} \frac{2\pi j}{\Gamma(1 + \sum_{i=1}^N n_i)} \quad (54)$$

Using (54) in (52), we apply the definition of N -Multivariate Fox's H-function in [55, A.1] to get (15) of Theorem 2.

We validate the derived PDF in (14) by $\int_0^\infty f_Z(z)dz = 1$. Using the parameters of \mathcal{F} -distributed atmospheric turbulence from Table II in (14), we use the definition of Fox's H-function and interchange the order of integration to solve the inner integral using the final value theorem: $\int_0^\infty x^{-1-\sum_{i=1}^N x_i} dz = \lim_{s \rightarrow 0} (\frac{1}{s})^{-\sum_{i=1}^N x_i} \Gamma(-\sum_{i=1}^N x_i)$. Thus, we get (53).

Then, we use [52] and apply standard mathematical procedure for getting the limit of a function at $s \rightarrow 0$ in (53) to get a simplified expression, which results into

$$\int_0^\infty f_Z(z)dz = \prod_{i=1}^N \prod_{j=1}^L \frac{\rho_{i,j}^2 v_{i,j}^{k_{i,j}}}{\Gamma(\alpha_F(i,j))\Gamma(\beta_F(i,j))} \frac{\Gamma(\beta_F(i,j))\Gamma(\alpha_F(i,j))\Gamma(\rho_{i,j}^2)\Gamma(v_{i,j})^{k_{i,j}}}{\Gamma(1 + \rho_{i,j}^2)\Gamma(1 + v_{i,j})^{k_{i,j}}} = 1 \quad (55)$$

REFERENCES

- [1] M. D. Renzo *et al.*, "Smart radio environments empowered by reconfigurable AI meta-surfaces: An idea whose time has come," *EURASIP J. Wireless Commun. Netw.*, vol. 2019, no. 129, May 2019.
- [2] E. Basar *et al.*, "Wireless communications through reconfigurable intelligent surfaces," *IEEE Access*, vol. 7, pp. 116753–116773, Aug. 2019.
- [3] M. A. ElMossallamy *et al.*, "Reconfigurable intelligent surfaces for wireless communications: Principles, challenges, and opportunities," *IEEE Trans. Cogn. Commun. Netw.*, vol. 6, no. 3, pp. 990–1002, May 2020.
- [4] Q. Wu *et al.*, "Intelligent reflecting surface aided wireless communications: A tutorial," *IEEE Trans. Commun.*, vol. 69, no. 5, pp. 3313–3351, Jan. 2021.
- [5] X. Yuan *et al.*, "Reconfigurable-intelligent-surface empowered wireless communications: Challenges and opportunities," *IEEE Wireless Commun.*, vol. 28, no. 2, pp. 136–143, Feb. 2021.
- [6] M. A. Khalighi and M. Uysal, "Survey on free space optical communication: A communication theory perspective," *IEEE Commun. Surveys Tuts.*, vol. 16, no. 4, pp. 2231–2258, June 2014.
- [7] P. Yang *et al.*, "6G wireless communications: Vision and potential techniques," *IEEE Network*, vol. 33, no. 4, pp. 70–75, July 2019.
- [8] S. Dang *et al.*, "What should 6G be?" *Nature Electronics*, vol. 3, no. 1, pp. 20–29, Jan. 2020.
- [9] M. Safari and M. Uysal, "Relay-assisted free-space optical communication," *IEEE Trans. Wirel. Commun.*, vol. 7, no. 12, pp. 5441–5449, Dec. 2008.
- [10] I. S. Ansari *et al.*, "Performance analysis of free-space optical links over Málaga (\mathcal{M}) turbulence channels with pointing errors," *IEEE Trans. Wirel. Commun.*, vol. 15, no. 1, pp. 91–102, Jan. 2016.
- [11] E. Zedini *et al.*, "Dual hop FSO transmission systems over Gamma Gamma turbulence with pointing errors," *IEEE Trans. Wirel. Commun.*, vol. 16, no. 2, pp. 784–796, Feb 2017.
- [12] Y. Zhang *et al.*, "On the performance of dual-hop systems over mixed FSO/mmWave fading channels," *IEEE Open J. Commun. Soc.*, vol. 1, pp. 477–489, April 2020.
- [13] D. Kudathanthirige *et al.*, "Performance analysis of intelligent reflective surfaces for wireless communication," in *2020 IEEE Int. Conf. Commun. (ICC)*, Dublin, Ireland, July 2020, pp. 1–6.
- [14] A. A. A. Boulogeorgos and A. Alexiou, "Ergodic capacity analysis of reconfigurable intelligent surface assisted wireless systems," in *2020 IEEE 3rd 5G World Forum (5GWF)*, Bangalore, India, Oct. 2020, pp. 395–400.
- [15] A.-A. A. Boulogeorgos and A. Alexiou, "Performance analysis of reconfigurable intelligent surface-assisted wireless systems and comparison with relaying," *IEEE Access*, vol. 8, pp. 94463–94483, May 2020.
- [16] L. Yang *et al.*, "Accurate closed-form approximations to channel distributions of RIS-aided wireless systems," *IEEE Wireless Commun. Lett.*, vol. 9, no. 11, pp. 1985–1989, July 2020.
- [17] Q. Tao *et al.*, "Performance analysis of intelligent reflecting surface aided communication systems," *IEEE Commun. Lett.*, vol. 24, no. 11, pp. 2464–2468, July 2020.
- [18] R. C. Ferreira *et al.*, "Bit error probability for large intelligent surfaces under double-Nakagami fading channels," *IEEE Open J. Commun. Society*, vol. 1, pp. 750–759, May 2020.
- [19] D. Selimis *et al.*, "On the performance analysis of RIS-empowered communications over Nakagami-m fading," *IEEE Commun. Lett.*, vol. 25, no. 7, pp. 2191–2195, April 2021.
- [20] H. Ibrahim *et al.*, "Exact coverage analysis of intelligent reflecting surfaces with Nakagami-m channels," *IEEE Trans. Veh. Technol.*, vol. 70, no. 1, pp. 1072–1076, Jan. 2021.
- [21] I. Trigui *et al.*, "A comprehensive study of reconfigurable intelligent surfaces in generalized fading," [Online], arXiv: 2004.02922, 2020.
- [22] H. Du *et al.*, "Millimeter wave communications with reconfigurable intelligent surfaces: Performance analysis and optimization," *IEEE Trans. Commun.*, vol. 69, no. 4, pp. 2752–2768, Jan. 2021.
- [23] L. Yang *et al.*, "Indoor mixed dual-hop VLC/RF systems through reconfigurable intelligent surfaces," *IEEE Wireless Commun. Lett.*, vol. 9, no. 11, pp. 1995–1999, July 2020.
- [24] —, "Mixed dual-hop FSO-RF communication systems through reconfigurable intelligent surface," *IEEE Commun. Lett.*, vol. 24, no. 7, pp. 1558–1562, April 2020.
- [25] A. Sikri *et al.*, "Reconfigurable intelligent surface for mixed FSO-RF systems with co-channel interference," *IEEE Commun. Lett.*, vol. 25, no. 5, pp. 1605–1609, Feb. 2021.
- [26] V. Jamali *et al.*, "Intelligent reflecting surface assisted free-space optical communications," *IEEE Commun. Magazine*, vol. 59, no. 10, pp. 57–63, Nov. 2021.
- [27] M. Najafi and R. Schober, "Intelligent reflecting surfaces for free space optical communications," in *2019 IEEE Global Commun. Conference (GLOBECOM)*, Waikoloa, HI, USA, Dec. 2019, pp. 1–7.
- [28] H. Wang *et al.*, "Performance of wireless optical communication with reconfigurable intelligent surfaces and random obstacles," arXiv:2001.05715, 2020.
- [29] L. Yang *et al.*, "Free-space optical communication with reconfigurable intelligent surfaces," arXiv: 2012.00547, 2020.
- [30] A. R. Ndjiongue *et al.*, "Performance analysis of RIS-based nT-FSO link over \mathcal{G} - \mathcal{G} turbulence with pointing errors," arXiv: 2102.03654, 2021.
- [31] Z. Cao *et al.*, "Reconfigurable beam system for non-line-of-sight free-space optical communication," *Light Sci Appl*, vol. 3, no. 1, pp. 20–29, July 2019.

- [32] M. Al-Habash *et al.*, “Mathematical model for the irradiance probability density function of a laser beam propagating through turbulent media,” *Opt. Eng.*, vol. 40, pp. 1554–1562, Aug. 2001.
- [33] A. Jurado-Navas *et al.*, “A unifying statistical model for atmospheric optical scintillation,” *Numerical Simulations of Physical and Engineering Processes*, Sep 2011.
- [34] K. P. Peppas *et al.*, “The Fischer–Snedecor \mathcal{F} -distribution model for turbulence-induced fading in free-space optical systems,” *J. Lightw. Technol.*, vol. 38, no. 6, pp. 1286–1295, March 2020.
- [35] A. A. Farid and S. Hranilovic, “Outage capacity optimization for free-space optical links with pointing errors,” *J. Lightw. Technol.*, vol. 25, no. 7, pp. 1702–1710, July 2007.
- [36] I. I. Kim *et al.*, “Comparison of laser beam propagation at 785 nm and 1550 nm in fog and haze for optical wireless communications,” *Proc. SPIE*, vol. 4214, pp. 26–37, Nov. 2001.
- [37] M. A. Esmail *et al.*, “On the performance of optical wireless links over random foggy channels,” *IEEE Access*, vol. 5, pp. 2894–2903, Feb. 2017.
- [38] L. Kong *et al.*, “Effective rate evaluation of RIS-assisted communications using the sums of cascaded α - μ random variates,” *IEEE Access*, vol. 9, pp. 5832–5844, Jan. 2021.
- [39] H. Du *et al.*, “Reconfigurable intelligent surface aided TeraHertz communications under misalignment and hardware impairments,” [Online] arXiv: 2012.00267, 2020.
- [40] V. K. Chapala and S. M. Zafaruddin, “Exact Analysis of RIS-Aided THz Wireless Systems Over α - μ Fading with Pointing Errors,” *IEEE Commun. Lett.*, vol. 25, no. 11, pp. 3508–3512, Nov. 2021.
- [41] C. Huang *et al.*, “Reconfigurable intelligent surfaces for energy efficiency in wireless communication,” *IEEE Trans. Wirel. Commun.*, vol. 18, no. 8, pp. 4157–4170, June 2019.
- [42] P. Xu *et al.*, “Ergodic secrecy rate of RIS-assisted communication systems in the presence of discrete phase shifts and multiple eavesdroppers,” *IEEE Wireless Commun. Lett.*, vol. 10, no. 3, pp. 629–633, March 2021.
- [43] F. Yang *et al.*, “Free-space optical communication with nonzero bore-sight pointing errors,” *IEEE Trans. Commun.*, vol. 62, no. 2, pp. 713–725, Feb. 2014.
- [44] R. Boluda-Ruiz *et al.*, “Novel approximation of misalignment fading modeled by Beckmann distribution on free-space optical links,” *Opt. Express*, vol. 24, no. 20, pp. 22 635–22 649, Oct 2016.
- [45] K.-J. Jung *et al.*, “Unified finite series approximation of FSO performance over strong turbulence combined with various pointing error conditions,” *IEEE Trans. Commun.*, vol. 68, no. 10, pp. 6413–6425, Oct. 2020.
- [46] H. G. Sandalidis *et al.*, “BER performance of FSO links over strong atmospheric turbulence channels with pointing errors,” *IEEE Commun. Lett.*, vol. 12, no. 1, pp. 44–46, Jan. 2008.
- [47] O. Badarneh *et al.*, “Performance analysis of FSO communications over (\mathcal{F}) turbulence channels with pointing errors,” *IEEE Commun. Lett.*, vol. 3, pp. 926–930, Dec. 2020.
- [48] Z. Rahman *et al.*, “Performance of opportunistic beam selection for ovc system under foggy channel with pointing error,” *IEEE Commun. Lett.*, vol. 24, no. 9, pp. 2029–2033, Sept. 2020.
- [49] —, “Performance of dual-hop relaying for OWC system over foggy channel with pointing errors and atmospheric turbulence,” arXiv 2105.14256: 2021.
- [50] A. Papoulis and U. Pillai, *Probability, random variables and stochastic processes*, 4th ed. McGraw-Hill, Nov. 2001.
- [51] L. Huang *et al.*, “Unified Performance Analysis of Hybrid FSO/RF System With Diversity Combining,” *Journal of Lightwave Technology*, vol. 38, no. 24, pp. 6788–6800, Dec. 2020.
- [52] Y. Abo Rahama *et al.*, “On the sum of independent Fox’s H -function variates with applications,” *IEEE Trans. Vehi. Technol.*, vol. 67, no. 8, pp. 6752–6760, Aug. 2018.
- [53] *The Wolfram function Site*, Accessed May 2021: <https://functions.wolfram.com/>.
- [54] I. S. Ansari *et al.*, “A new formula for the BER of binary modulations with dual-branch selection over generalized-K composite fading channels,” *IEEE Trans. Commun.*, vol. 59, no. 10, pp. 2654–2658, Oct. 2011.
- [55] A. Mathai *et al.*, *The H-Function: Theory and Applications*. Springer New York, 2009.
- [56] H. R. Alhennawi *et al.*, “Closed-form exact and asymptotic expressions for the symbol error rate and capacity of the H -function fading channel,” *IEEE Trans. Vehi. Technol.*, vol. 65, no. 4, pp. 1957–1974, April 2016.
- [57] W. Gappmair, “Further results on the capacity of free-space optical channels in turbulent atmosphere,” *IET Commun.*, vol. 5, p. 1262 – 1267, July 2011.
- [58] I. Gradshteyn *et al.*, *Table of Integrals, Series, And Products*. Elsevier Academic Press, 2007.
- [59] N. Hai and H. Srivastava, “The convergence problem of certain multiple Mellin-Barnes contour integrals representing H -functions in several variables,” *Computers & Mathematics With Applications*, vol. 29, pp. 17–25, 1995.



Vinay Kumar Chapala received the B.Tech degree in Electronics and Communication Engineering from Jawaharlal Nehru Technology University, Hyderabad in 2010 and the M.Tech degree in Communications Engineering from Indian Institute of Technology, Delhi in 2013. He is a Staff Engineer with Qualcomm India Pvt Ltd, Bangalore. He is currently pursuing the PhD degree in communication systems with the Department of Electrical and Electronics Engineering, Birla Institute of Technology and Science at Pilani, Pilani, India. His current research interests include signal processing and machine learning for wireless communications, and reconfigurable intelligent surfaces for wireless systems.



S. M. Zafaruddin (Senior Member, IEEE) received the Ph.D. degree in electrical engineering from IIT Delhi, New Delhi, India, in 2013. From 2012 to 2015, he was with Ikanos Communications (now Qualcomm), Bangalore, India, working directly with the CTO Office, Red Bank, NJ, USA, where he was involved in research and development for xDSL systems. From 2015 to 2018, he was a Post-Doctoral Researcher with the Faculty of Engineering, Bar-Ilan University, Ramat Gan, Israel, where he was involved in signal processing for wireline and wireless communications. He is currently an Assistant Professor with the Department of Electrical and Electronics Engineering, Birla Institute of Technology and Science at Pilani, Pilani, India. His current research interests include signal processing and machine learning for wireless and wireline communications, THz wireless technology, optical wireless communications, reconfigurable intelligent surface, distributed signal processing, and resource allocation algorithms. He received the Planning and Budgeting Commission Fellowship for Outstanding Post-Doctoral Researchers from China and India by the Council for Higher Education, Israel (2016–2018). He is also an Associate Editor of the IEEE ACCESS.